

Minkowski Tensors of Anisotropic Spatial Structure

G.E. Schröder-Turk^{1,*}, W. Mickel^{1,2}, S.C. Kapfer¹,
F.M. Schaller¹, B. Breidenbach¹, D. Hug², and K. Mecke¹

¹ Theoretische Physik, Friedrich-Alexander-Universität Erlangen-Nürnberg,
Staudtstr. 7B, D-91058 Erlangen, Germany

² Karlsruhe Institute of Technology, Institute for Stochastics, Kaiserstr. 89-93,
D-76128 Karlsruhe, Germany

Abstract. This article describes the theoretical foundation of and explicit algorithms for a novel approach to morphology and anisotropy analysis of complex spatial structure using tensor-valued Minkowski functionals, the so-called *Minkowski tensors*. Minkowski tensors are generalisations of the well-known scalar Minkowski functionals and are explicitly sensitive to anisotropic aspects of morphology, relevant for example for elastic moduli or permeability of microstructured materials. Here we derive explicit linear-time algorithms to compute these tensorial measures for three-dimensional shapes. These apply to representations of any object that can be represented by a triangulation of its bounding surface; their application is illustrated for the polyhedral Voronoi cellular complexes of jammed sphere configurations, and for triangulations of a biopolymer fibre network obtained by confocal microscopy. The article further bridges the substantial notational and conceptual gap between the different but equivalent approaches to scalar or tensorial Minkowski functionals in mathematics and in physics, hence making the mathematical measure theoretic method more readily accessible for future application in the physical sciences.

The morphology of complex spatial microstructures is often classified qualitatively into types such as cellular, porous, network-like, fibrous, percolating, periodic, lamellar, hexagonal, disordered, fractal, etc. Various quantitative measures of morphology have been defined often applicable to one specific type only, for example moments of the distributions of angles of tangent vectors with a fixed specified direction as anisotropy characterisation of a network structure. Apart from the concept of correlation functions, few measures are defined sensibly and robustly for all types. In this article, we describe the class of Minkowski tensors (MT) that apply generically to almost any type of structure which contains two or more phases separated by a well-defined interface, for example, porous media, foams, trabecular bone, granular material. The MT are defined as integrals of powers of normal and position vectors and surface curvatures, or curvature measures. Because of their tensorial nature they are explicitly sensitive to anisotropic and orientational aspects of spatial structure. Figure 1 shows examples of systems where subtle anisotropy of the spatial structure influences the physical properties and to which the analysis of this article is applicable.

The scope of this article is the thorough theoretical description of the MT approach to spatial structure analysis and the derivation of a robust algorithm to compute MT

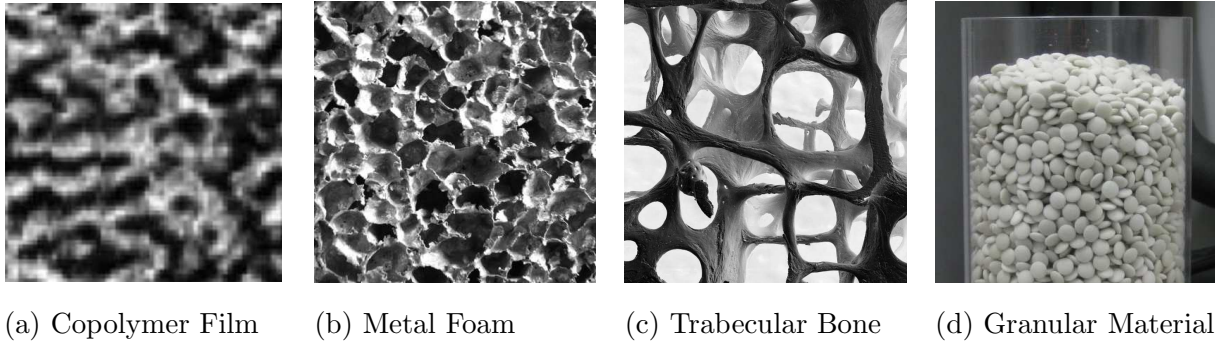


Figure 1. Examples of systems with anisotropic spatial structure. (a) A microphase-separated copolymer film aligns under the influence of an external electric field (image courtesy A. Böker and V. Oszowka, see also [8, 9]). (b) Closed-cell metal foam (image courtesy of M. Saadatfar [10]). (c) Structure of trabecular bone (image courtesy Alan Boyde [11]). (d) Packing of ellipsoids as a model system for anisotropic granular matter.

of bi-phasic materials. It will facilitate the use of tensorial Minkowski functionals as robust structure metrics for shape description and for structure-property correlations in physics and material science. It simultaneously provides the theoretic and algorithmic basis of our previous applications of this method [1, 2, 3, 4, 5, 6, 7], and broadens the scope of the MT concept. A secondary purpose is to bridge the gap between the notation and concepts commonly used in the physics literature for scalar Minkowski functionals, based on surface and volume integrals, and the integral geometry literature, where both scalar and tensorial Minkowski functionals are derived based on measure theory.

Minkowski tensors are direct generalisations of scalar-valued Minkowski functionals (MF). These latter are well established as succinct descriptors of morphology and spatial structure for various physical processes [12]. These integral geometric measures have been applied to disordered porous materials [13] and are relevant to flow phenomena therein [14, 15], to nano-scale microstructures in copolymers [16], to the dewetting dynamics of thin films [17], and to Turing patterns [18]. They have also been shown to be the most pertinent morphological quantities on which the thermodynamic properties of simple fluids near curved solid interfaces depend [19, 20]. The mathematical theory of MF and their generalisations has been comprehensively developed in the context of integral geometry [21, 22, 23, 24], with several aspects shared also with the discipline of mathematical morphology [25, 26, 27].

MF as scalar quantities are not sensitive to features of the morphology which relate to orientation or directional anisotropy, since motion-invariance is one of their defining properties. Therefore scalar MF do not provide quantification of anisotropy that is relevant to study the direction-dependence of physical processes, such as elastic properties or permeability of anisotropic porous or microstructured materials or systems with external fields. This motivates their generalisation to tensorial quantities. MT have

already been shown to be the relevant morphological descriptors for a density functional theory of fluids of non-spherical particles [28] and of DNA conformations [29], and of a simple model for transport with molecular motors [30]. They have also been used, in 2D, as morphology descriptors of arrangements of neuronal cells [31], galaxies [32], and Turing patterns [6].

The mathematical discipline of integral geometry has proven statements regarding continuity and completeness similar to the Hadwiger theorem in the scalar case [33, 34, 35, 36]. However, an algorithm for the computation of the MT applicable to experimental 3D data – a prerequisite for their use as shape indices for experimental data – has thus far been lacking. (Note that the work in refs. [1, 2, 3, 4, 5, 6, 7, 5] has employed the algorithms described in this article without thorough comprehensive description.)

A primary application of rank-2 MT is the quantitative analysis of the degree of intrinsic anisotropy of materials with complex spatial structure. Scalar measures of anisotropy are easily derived as eigenvalue ratios of the MT. Evidently, alternative methods for the characterisation of anisotropy and alignment exist. Fourier transforms are a common way to characterise anisotropy, and have been applied e.g. for trabecular bone [37], for electrodeposited patterns [38], for fibre systems [39], and for structured polyethylene mats [40]. Related methods based on correlation functions are also known [41, 42]. Fourier methods that analyse the amplitude of the Fourier transform of a gray-scale image in polar coordinates can also quantify alignment, e.g. of copolymer films in electric fields [8]. Anisotropy indices derived from the normal vector distribution of a given shape, similar to the MT, have been used to describe the shape anisotropy of simulated 3D foam cells [43, 44] and liquid interfaces [45, 3]. An anisotropy measure applicable to porous media is derived from the directional variations of average chord lengths. For a binary composite, i.e. consisting of a solid and a void phase, a chord is a segment of an infinite straight line that is fully contained in one of the two phases. Analyses of chord lengths and the derived mean intercept length ellipsoid are used for the investigation of the microstructure of bone [46, 47, 48, 49, 50, 51], see also ref. [52] for a comparison of anisotropy measures based on mean-intercept length, star-volume and star-length distributions. Deformations of cellular or granular material have recently been quantified using the so-called *texture tensor* C , defined as the sum $C_{ij} := \sum l_i l_j$ over a subset of link vectors \mathbf{l} in the structure [53, 54]. The texture tensor can be used to characterise anisotropy, e.g. for Antarctic ice crystals [55] and liquid foam cells [56]. Further anisotropy measures are based on the Steiner compact [57], wavelet analysis [58], the orientation of volumes [59] or star-volumes [60]. Two-dimensional equivalents of the anisotropy measures discussed in this article have previously been used for the analysis of the shape of neuronal cells [31] and galaxies [32], and are discussed in detail in [6].

The paper is organised as follows: Section 1 provides an overview of the theory of MF and MT, based on their definition by surface integrals which is widely used in the physical sciences. To bridge the gap in notation between the physics and the

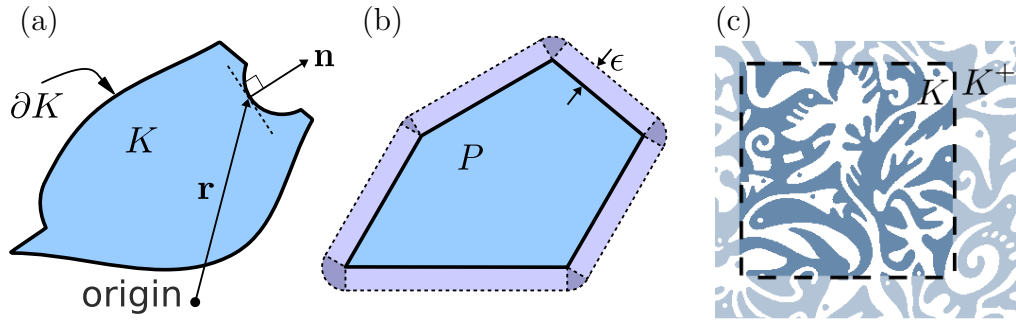


Figure 2. (a) A body K with bounding surface ∂K ; (b) a convex polytope P and its parallel body (or dilation) $P \uplus B_\epsilon$; (c) a subset of a topologically more complex body based on Craig Marlow’s painting “White Spirits” [61]. The latter demonstrates a common experimental situation, namely that the given body K represents a finite subset of a larger body K^+ , here the body K clipped to the *window of observation* T , $K = K^+ \cap T$. K is assumed to be a representative subset of the larger body, which allows for the estimation of intrinsic shape features of K^+ . If only K , but not K^+ , is available for analysis particular care must be taken w.r.t. those bounding surface patches of K that result purely from taking the subset, i.e. those that are on the boundaries of the window of observation.

mathematics literature this section also includes a discussion of the alternative definition based on measure theory. Section 2 derives algorithms to compute MT for bodies represented by triangulations of their bounding surface; their implementation is provided as supplementary online material to this article. Section 3 describes anisotropy measures derived from the MT and illustrates their application to two experimental data sets. The appendix provides analytic expressions for the MT for some simple geometric shapes.

1. Definition and fundamental properties

Scalar MF and MT can be used as shape measures to quantify the shape or form of an object. They can be defined in two largely equivalent ways. In the physical sciences, a definition based on curvature-weighted integrals of position or surface normal vectors over the object’s bounding surface has been popular for the scalar MF, and forms the basis of the numerical algorithms derived in this article. An alternative, more fundamental definition is provided by the measure theoretic approach of integral geometry (see 1.2).

The object, also referred to as *body*, whose shape can be characterised by MT or MF is denoted by K . Assuming that K is a compact set with nonempty interior embedded in Euclidean space \mathbb{R}^3 and is bounded by a sufficiently smooth surface ∂K , we define MF of K as

$$W_0(K) = \int_K dV \quad \text{and} \quad W_\nu(K) = \frac{1}{3} \int_{\partial K} G_\nu dA \quad (1)$$

in space-dimension $d = 3$ and with $\nu = 1, 2, 3$. The scalar functions G_ν are $G_1 = 1$, the mean curvature $G_2 = (k_1 + k_2)/2$ and the Gaussian curvature $G_3 = k_1 \cdot k_2$ of the bounding surface ∂K ; the scalars k_1, k_2 are the principal curvatures on ∂K as defined in differential geometry, dV is the infinitesimal volume and dA the scalar infinitesimal area element. This definition naturally applies to both convex and non-convex bodies of arbitrary topology with a sufficiently smooth bounding surface. The prefactor is chosen such that for a sphere B_R with radius R the scalar MF are $W_\nu(B_R) = \kappa_3 R^{3-\nu}$ where $\kappa_3 = 4\pi/3$ is the volume of the 3-dimensional unit sphere ‡.

The MF W_2 and W_3 (in 3D space) are not properly defined by eq. (1) for bodies with sharp edges or corners, due to singularities of the mean and Gaussian curvatures G_2 and G_3 . However, for convex bodies, consideration of a parallel or dilated body in the limit of vanishing thickness provides a robust definition, by use of the Steiner formula. The Steiner formula states that, for a given convex body K , the MF of the parallel or dilated body $(K \uplus B_\epsilon)$ are a polynomial in $\epsilon \geq 0$ with coefficients proportional to the MF of K ; for $\epsilon > 0$, $K_\epsilon := K \uplus B_\epsilon := \{\mathbf{x}_1 + \mathbf{x}_2 : \mathbf{x}_1 \in K, \mathbf{x}_2 \in B_\epsilon\}$ is the parallel or dilated body of K (see Fig. 2). Specifically for the volume one finds $W_0(K \uplus B_\epsilon) = W_0(K) + 3W_1(K)\epsilon + 3W_2(K)\epsilon^2 + W_3(K)\epsilon^3$, and more generally

$$W_\nu(K \uplus B_\epsilon) = \sum_{\mu=\nu}^3 \binom{3-\nu}{\mu-\nu} W_\mu(K) \epsilon^{\mu-\nu}. \quad (2)$$

Sharp edges and vertices of K correspond to cylindrical or spherical segments on the bounding surface $\partial(K \uplus B_\epsilon)$ of the parallel or dilated body. The bounding surface is sufficiently smooth for $\epsilon > 0$ and $W_\nu(K \uplus B_\epsilon)$ converges to $W_\nu(K)$ in the limit $\epsilon \rightarrow 0$. It is further necessary to define MF and MT for certain non-convex bodies, with or without positive reach, see e.g. [24, Note 1 to Section 5.3 and refs. therein]; this is achieved below by exploiting an additivity relationship. A further discussion for non-smooth bodies can be found in section 2.

MT are symmetric tensors (that is, invariant under index permutation), which are generated by symmetric tensor products of position vectors \mathbf{x} and normal vectors \mathbf{n} of ∂K . The dyadic (or tensor) product of two vectors \mathbf{a} and \mathbf{b} is $(\mathbf{a} \otimes \mathbf{b})_{ij} := \mathbf{a}_i \mathbf{b}_j$. Let now \mathbf{a} and \mathbf{b} be symmetric tensors of rank r and s , respectively. The symmetric tensor product is defined as

$$(\mathbf{a} \odot \mathbf{b})_{i_1 \dots i_{r+s}} := \frac{1}{(r+s)!} \sum_{\sigma \in S_{r+s}} \mathbf{a}_{i_{\sigma(1)}} \dots \mathbf{a}_{i_{\sigma(r)}} \mathbf{b}_{i_{\sigma(r+1)}} \dots \mathbf{b}_{i_{\sigma(r+s)}}, \quad (3)$$

where S_{r+s} is the permutation group of $r+s$ elements. For two tensors \mathbf{a} and \mathbf{b} , we use

‡ Other normalisations of the scalar MF are also common in the literature. The kinematic formulae [23, 24] have particularly simple coefficients if the normalisation $M_\nu(K) = \kappa_{d-\nu} W_\nu(K) / (\kappa_\nu \kappa_d)$ is used, with the volume of the n -dimensional unit ball $\kappa_n := \pi^{n/2} / \Gamma(n/2 + 1)$. In the mathematical literature, in d -dimensional Euclidean space the normalisation $V_{d-\nu}(K) = \binom{d}{\nu} W_\nu(K) / \kappa_\nu$ is frequently used, and the $V_{d-\nu}$ are called the *intrinsic volumes* of K . In three dimensions, the set of MF thus consists of the volume $W_0 = M_0 = V_3$, the surface area $3W_1 = 8M_1 = 2V_2$, the integrated mean curvature $3W_2 = 2\pi^2 M_2 = \pi V_1$, and the Euler characteristic $\chi = \frac{3}{4\pi} W_3 = \frac{4\pi}{3} M_3 = V_0$ with $\chi(B_R) = 1$.

the shorter notation $\mathbf{a}^2 := \mathbf{a} \odot \mathbf{a} = \mathbf{a} \otimes \mathbf{a}$ and $\mathbf{ab} := \mathbf{a} \odot \mathbf{b}$. For example, if \mathbf{a} and \mathbf{b} are both vectors, the symmetric tensor product is the tensor \mathbf{ab} of rank 2.

The MT of rank two are defined as

$$W_0^{2,0}(K) := \int_K \mathbf{x}^2 \, dV \quad (4)$$

$$W_\nu^{r,s}(K) := \frac{1}{3} \int_{\partial K} G_\nu \mathbf{x}^r \mathbf{n}^s \, dA. \quad (5)$$

with $\nu = 1, 2, 3$ and $(r, s) = (2, 0), (1, 1)$ or $(0, 2)$. For ease of notation, we set $W_0^{r,s} := 0$ for $s > 0$ and $W_\nu^{r,s} := 0$ if $\nu < 0$ or $\nu > 3$. For a three-dimensional body, this definition yields 10 MT, not counting the ones that vanish by definition for all bodies.

MT of rank one (called Minkowski vectors) are defined by $W_0^{1,0} := \int_K \mathbf{x} \, dV$ and by $W_\nu^{1,0} := \frac{1}{3} \int_{\partial K} \mathbf{x} \, dA$ for $\nu = 1, 2, 3$. The prefactors are chosen such that, for a sphere centred at \mathbf{C} , the so-called *curvature centroids* $W_\nu^{1,0}/W_\nu$ are equal to \mathbf{C} . Note specifically that $W_1^{1,0}/W_0$ is the centre of mass (assuming a solidly filled body of constant density). Formally, vectors $W_\nu^{0,1}$ proportional to $\int_{\partial K} \mathbf{n} \, dA$ for $\nu = 1, 2, 3$ are also defined, however they vanish for any body with a closed bounding surface [35].

MT are isometry covariant, that is their behaviour under translations and rotations is given by

$$W_\nu^{r,s}(K \uplus \mathbf{t}) = \sum_{p=0}^r \binom{r}{p} \mathbf{t}^p W_\nu^{r-p,s}(K) \quad (6)$$

$$W_\nu^{r,s}(UK) = \hat{U}_{r+s} : W_\nu^{r,s}, \quad (7)$$

where $K \uplus \mathbf{t}$ is the translation of K by the vector \mathbf{t} , UK is a rotated copy of K , and \hat{U}_{r+s} denotes the corresponding rotation tensor for a rank- $(r+s)$ tensor:

$$\left(\hat{U}_{r+s} : W_\nu^{r,s} \right)_{i_1, \dots, i_{r+s}} := \sum_{j_1, \dots, j_{r+s}} U_{i_1, j_1} \dots U_{i_{r+s}, j_{r+s}} (W_\nu^{r,s})_{j_1, \dots, j_{r+s}}. \quad (8)$$

In this expression, U_{ij} is the conventional orthogonal 3×3 transformation matrix associated with the rotation U .

For $r = 0$, equation (6) gives $W_\nu^{r,s}(K) = W_\nu^{r,s}(K \uplus \mathbf{t})$. A tensor that fulfils this relation for all K is called *translation invariant*. Genuinely translation covariant tensors fulfil eq. (6) but not the translation invariance condition. For the sake of brevity, we will use the term *translation covariant* to denote specifically the genuinely translation covariant tensors. All $W_\nu^{0,s}$ are translation invariant by their definition; in dimension $d = 3$, also the tensors $W_1^{1,1}$, $W_2^{1,1}$ and $W_3^{1,1}$ are translation invariant due to the envelope theorems of Müller [35]. Translation invariance is important whenever a natural choice for the origin is not available.

All MF and MT are homogeneous, i.e. they fulfil the homogeneity relation $W_\nu^{r,s}(\lambda K) = \lambda^{3+r-\nu} W_\nu^{r,s}(K)$. Table 1 specifies the translation and homogeneity behaviour of the MF and MT.

Homogeneity [unit]	rank 0	rank 1	rank 2	translation behaviour
$\lambda^5 [m^5]$	–	–	$W_0^{2,0}$	genuinely translation covariant
$\lambda^4 [m^4]$	–	$W_0^{1,0}$	$W_1^{2,0}$	genuinely translation covariant
$\lambda^3 [m^3]$	–	$W_1^{1,0}$	$W_2^{2,0}$	genuinely translation covariant
	W_0	–	$W_0 Q$	translation invariant
$\lambda^2 [m^2]$	–	$W_2^{1,0}$	$W_3^{2,0}$	genuinely translation covariant
	–	–	$W_1^{0,2}$	translation invariant
	W_1	–	$W_1 Q$	translation invariant
$\lambda^1 [m^1]$	–	$W_3^{1,0}$	–	genuinely translation covariant
	–	–	$W_2^{0,2}$	translation invariant
	W_2	–	$W_2 Q$	translation invariant
$\lambda^0 [1]$	W_3	–	$W_3 Q$	translation invariant

Table 1. Basic tensor valuations in 3D. The Minkowski functionals (scalars, rank 0) are motion invariant, the Minkowski vectors (rank 1) are genuinely translation covariant. For rank two, the space of Minkowski tensors decomposes into two complementary subspaces according to translation behaviour (indicated by the last column): genuinely translation covariant and translation invariant tensors. The latter include tensors obtained by multiplying the scalar MF W_ν with the unit tensor $Q := \mathbf{e}_1^2 + \mathbf{e}_2^2 + \mathbf{e}_3^2$ of rank two, where $\mathbf{e}_1, \mathbf{e}_2, \mathbf{e}_3$ are vectors of an orthonormal basis of \mathbb{R}^3 .

Thus far, MT have been defined for (a) convex or non-convex bodies with a smooth bounding surface and (b) convex bodies which may have sharp corners and edges. The case of non-convex bodies with concave sharp corners or edges cannot be treated by the parallel body construction (“dilation”) without further assumptions (technically, such bodies do not represent *sets of positive reach* [24, 62]). An extension of the definition of MF and MT to finite unions of convex bodies is achieved by exploiting a property called *additivity*

$$W_\nu^{r,s}(K \cup K') = W_\nu^{r,s}(K) + W_\nu^{r,s}(K') - W_\nu^{r,s}(K \cap K'), \quad (9)$$

if K, K' are all convex. In general, the union $(K \cup K')$ of two arbitrary convex bodies K and K' is not convex while the intersection $(K \cap K')$ is convex. Since $W_\nu^{r,s}$ are continuous functionals on convex bodies, eq. (9) can be used (see Groemer’s extension theorem [24]) to define the MF and MT for bodies that are unions of a finite number of convex bodies (such sets are called polyconvex).

MT of rank $(r + s)$ with $r + s > 1$ are *not* completely linearly independent, i.e. they do not contain independent shape information [34, 63]. For rank-2 MT and $d = 3$ the

linear dependencies

$$QW_\nu(K) = \nu W_\nu^{0,2}(K) + (3 - \nu)W_{\nu+1}^{1,1}(K) \quad (10)$$

are valid for any polyconvex body K in \mathbb{R}^3 and $\nu = 0, 1, 2, 3$; Q is the unit tensor of rank 2. In particular, it follows that $QW_3 = 3W_3^{0,2}$. Specifically, for $\nu = 0$ one obtains a special case of the Gauss' theorem

$$QW_0 = 3W_1^{1,1} \implies W_0 = \text{tr } W_1^{1,1}. \quad (11)$$

These relations are special cases of [34, eq. (1.1)] or [63, eq. (1.5)].

Alesker's theorem [33] makes a strong statement about the completeness of the MT for the purpose of shape description. For the special case of tensors of rank two, it states that any isometry covariant, additive, continuous functional φ on general convex bodies in \mathbb{R}^3 , taking values in the space of symmetric tensors of rank two over \mathbb{R}^3 , is a linear combination of the basic tensor valuations (an additive functional is called *valuation*) $Q^p W_\nu^{r,s}$, that is

$$\varphi(K) = \sum_{\nu,r,s,p} \varphi_\nu^{r,s,p} Q^p W_\nu^{r,s}(K) \quad (12)$$

with real coefficients $\varphi_\nu^{r,s,p}$ that do not depend on the convex body K [34, p. 150]. The coefficients $\varphi_\nu^{r,s,p}$ vanish unless $r + s + 2p = 2$. Starting from eq. (12) and using the linear dependencies among the basic tensor valuations, φ can be expressed in terms of linearly independent basic tensor valuations which form a basis of the corresponding vector space. The vector space of continuous, isometry covariant tensor valuations of rank two in \mathbb{R}^3 has dimension 10. A particular basis of this vector space consists of the six tensor valuations $W_0^{2,0}$, $W_1^{2,0}$, $W_2^{2,0}$, $W_3^{2,0}$, $W_1^{0,2}$ and $W_2^{0,2}$, which contain pertinent independent shape information, and of the four tensor valuations QW_ν , $\nu = 0, \dots, 3$. A summary is provided in Table 1.

Since φ is continuous and additive on convex bodies, it can be extended as an additive functional to finite unions of convex bodies. For this additive extension, eq. (12) remains valid since the right-hand side is a linear combination of additive functionals. It should be emphasised, however, that although all of these functionals are continuous on the space of convex bodies, they are not continuous on the space of finite unions of convex bodies, see the example in [6, Fig. 3].

1.1. MT of convex polytopes

It is instructive to illustrate the MT for convex polytopes P and to point out similarities to the tensor of inertia. We use here the letter P , rather than K , to denote a body whose bounding surface is a polytope, i.e. consisting of piece-wise linear facets. For a polytope, the tensors $W_\nu^{2,0}$ characterise the distribution of mass if the cell is a solid cell ($W_0^{2,0}$), a hollow cell ($W_1^{2,0}$), a wire frame ($W_2^{2,0}$) and a cell consisting of points at the vertices only ($W_3^{2,0}$); in the last two cases, however, this distribution of mass is weighted with certain exterior angles (see Fig. 3).

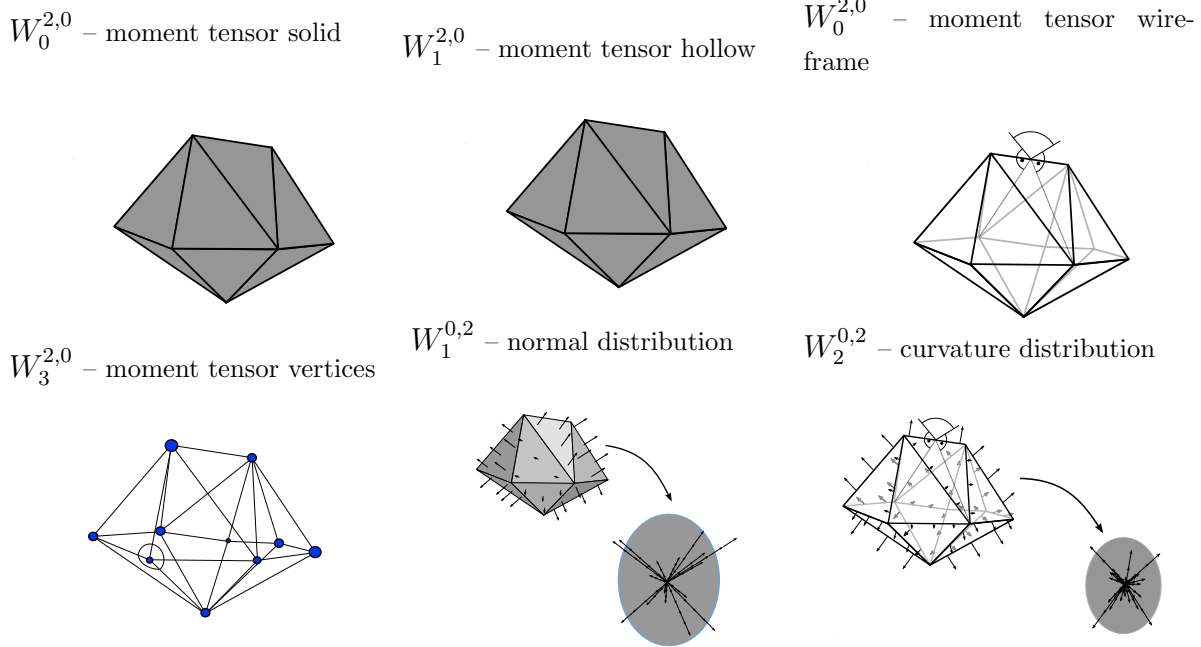


Figure 3. Interpretations of the Minkowski tensors for a polytope P : (a) Assuming homogeneous density, $W_2^{2,0}$ is the mass distribution tensor. (b-d) Contributions to surface-integrated moment tensors $W_\nu^{2,0}$ with $\nu = 1, \dots, 3$ are concentrated on $(3 - \nu)$ -dimensional surfaces. (e-f) Moments of the normal distribution on ∂P . Contributions to normal moment tensors $W_\nu^{0,2}$ with $\nu = 1, \dots, 2$ are also concentrated on $(3 - \nu)$ -dimensional surfaces. (reproduced from ref. [4])

The tensor of inertia \mathbb{I} , defined by $\mathbb{I}_{ij} = \int_K (-\mathbf{x}_i \mathbf{x}_j + \delta_{ij} |\mathbf{x}|^2) dV$, is a measure of the mass distribution of a (homogeneous) body K , relevant for the relationship between a rotation and the resulting moment. As \mathbb{I} is not translation-covariant, it is not a linear combination of the MT. However the simple relationship $\mathbb{I}(K) = -W_0^{2,0}(K) + \text{tr}(W_0^{2,0}(K)) Q$ holds for arbitrary K ; as above Q is the unit tensor of rank two of \mathbb{R}^3 , also called *metric tensor*. This illustrates that $W_0^{2,0}(K)$ is a measure of the distribution of mass if K is a homogeneously filled solid, somewhat analogous to the tensor of inertia. Similarly, $W_1^{2,0}(K)$ characterises the mass distribution if K is hollow and bounded by an infinitesimally thin surface sheet. This interpretation of $W_0^{2,0}$ and $W_1^{2,0}$ is valid for bodies K bounded by arbitrary surfaces (not just polytopes).

For a polytope P , the tensor $W_2^{2,0}(P)$ reduces to a line integral over the edges of the polytope (as the mean curvature vanishes on the flat facets, see also section 2) and is hence related to a mass distribution if P is given by a wire frame with wires along the edges. However, imposed by the requirement of additivity, the weight of the wire cannot be uniform but must be proportional to the mean curvature along the edge (i.e. the dihedral angle). Similarly, the tensor $W_3^{2,0}(P)$ reduces to a sum of point contributions, as the Gaussian curvature G_3 of P vanishes except at the vertices of the given polytope P . Again due to the additivity requirement, these vertices need to be weighted with the Gaussian curvature G_3 .

1.2. Definition based on fundamental measure theory

This section describes the alternative (and in some sense more fundamental) definition of MF and MT based on integral geometry and fundamental measure theory. The purpose of this section is to bridge the gap between the mathematics and physics literature on MF and MT. However, its content is not required for the numerical approaches to MF and MT described in section 2.

In integral geometry, the definition of MF and MT is based on so-called *support measures* (sometimes called *generalised curvature measures*) that can be thought of as local versions of the scalar MF [21, 23, 64, 24].

If support measures are available, then the MT for convex (or more general) bodies are obtained by integrating tensor functions with respect to these measures. Here we describe the approach for convex sets. The idea underlying the introduction of support measures for convex sets is to generalise the notion of a parallel set (or “dilation”, see Fig. 4 for $d = 2$) of a convex body K in d -dimensional Euclidean space \mathbb{R}^d to a suitable local construction.

A definition of the local parallel set that also applies to convex bodies K without smooth boundary is given in the following: We define $\mathbf{p}_K(\mathbf{x})$ as the unique point in K which is nearest to a given point $\mathbf{x} \in \mathbb{R}^d$. This defines a continuous map $\mathbf{p}_K(\cdot) : \mathbb{R}^d \rightarrow K$, $\mathbf{x} \mapsto \mathbf{p}_K(\mathbf{x})$. Then $d_K(\mathbf{x}) := \|\mathbf{x} - \mathbf{p}_K(\mathbf{x})\|$ is the distance from \mathbf{x} to K and $\mathbf{n}_K(\mathbf{x}) := (\mathbf{x} - \mathbf{p}_K(\mathbf{x}))/d_K(\mathbf{x})$, for $\mathbf{x} \in \mathbb{R}^d \setminus K$, is an exterior unit normal of K at the boundary point $\mathbf{p}_K(\mathbf{x}) \in \partial K$ (see Fig. 4). This construction achieves a definition of nearest points (reminiscent of the Euclidean distance map [65]) and surface normals that is also well-defined for points \mathbf{x} whose nearest point on K is a sharp corner (where the tangent plane is not well-defined and hence the conventional differential geometric definition of the surface normal does not apply).

Now we shall derive a local Steiner formula and support measures, following ref. [24] to obtain local support measures. The definition of MF and MT then follows directly as a special case [34, 63]. The intuitive idea underlying the definition of a local parallel set is described in two steps. First, we specify a region $L \subset \mathbb{R}^d$ and some $\epsilon > 0$. Then we consider all points $\mathbf{x} \in \mathbb{R}^d \setminus K$ which have distance $d_K(\mathbf{x})$ at most ϵ from K and for which $\mathbf{p}_K(\mathbf{x}) \in L$. Second, if K has points (such as at sharp corners or edges) where the exterior surface unit normal vector is not unique, then it is natural to restrict the points in this local outer parallel set further by also requiring $\mathbf{n}_K(\mathbf{x})$ to lie in a prescribed set $S \subset \mathbb{S}^{d-1}$. As an example, consider the polytope P in Fig. 4 (b1); for the definition of the local parallel set (shaded dark) it is necessary to specify which angular fraction of the wedges should be part of the local parallel set. This motivates the definition of the local parallel set by specification of the spatial region L and by the subset $S \subset \mathbb{S}^{d-1}$ of normal directions, conveniently combined to $\eta = L \times S \subset \mathbb{R}^d \times \mathbb{S}^{d-1}$, where \mathbb{S}^{d-1} is the d -dimensional unit sphere. This two step procedure can be merged and slightly extended to the following general definition.

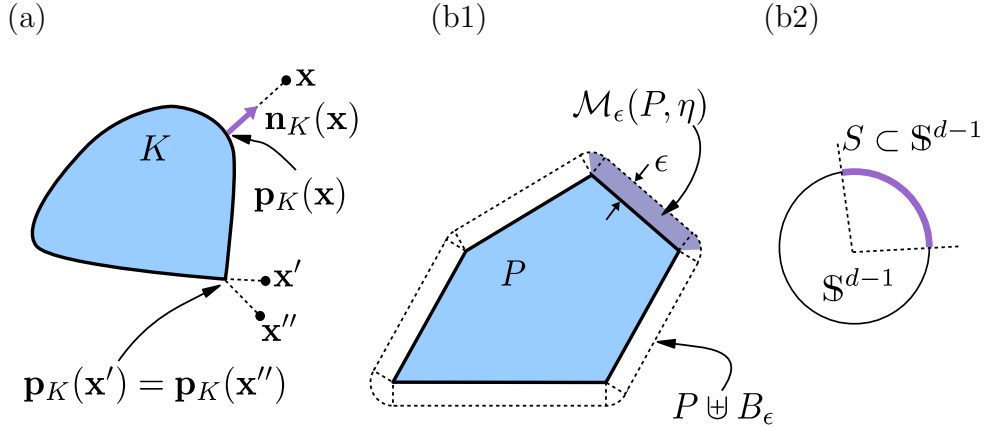


Figure 4. Construction of a local parallel set. (a) Definition of the normal field over an arbitrary convex body K at its boundary ∂K . (b1-b2) Local parallel set $\mathcal{M}_\epsilon(P, \eta)$ (illustrated for a polytope P) where only points are considered for which the normal direction is in a prescribed subset S of the unit sphere. (Here: $\eta = \mathbb{R}^d \times S$.)

For given $\epsilon > 0$ and $\eta \subset \mathbb{R}^d \times \mathbb{S}^{d-1}$, the local parallel set of K defined by

$$\mathcal{M}_\epsilon(K, \eta) := \{\mathbf{x} \in \mathbb{R}^d \setminus K : d_K(\mathbf{x}) \leq \epsilon, (\mathbf{p}_K(\mathbf{x}), \mathbf{n}_K(\mathbf{x})) \in \eta\} \quad (13)$$

contains all points $\mathbf{x} \in \mathbb{R}^d$ with $0 < d_K(\mathbf{x}) \leq \epsilon$ such that the pair $(\mathbf{p}_K(\mathbf{x}), \mathbf{n}_K(\mathbf{x})) \in \eta$. The first condition restricts \mathbf{x} to the global outer parallel set $(K \uplus B_\epsilon) \setminus K$ (see Fig. 4 (b1)). The second condition restricts $\mathcal{M}_\epsilon(K, \eta)$ to those points $\mathbf{x} \in \mathbb{R}^d$ of the global outer parallel set, where $(\mathbf{p}_K(\mathbf{x}), \mathbf{n}_K(\mathbf{x})) \in \eta$.

The volume of this local parallel set of a convex body K is $V_d(\mathcal{M}_\epsilon(K, \eta))$. A fundamental result in integral geometry, known as the *local Steiner formula* [64, 24], states that the map $\epsilon \mapsto V_d(\mathcal{M}_\epsilon(K, \eta))$ for all $\epsilon > 0$ (V_d is the d -dimensional Lebesgue-measure) is a polynomial of degree d , that is

$$V_d(\mathcal{M}_\epsilon(K, \eta)) = \sum_{\nu=0}^{d-1} \epsilon^{d-\nu} \kappa_{d-\nu} \Lambda_\nu(K, \eta), \quad (14)$$

where $\kappa_n := \pi^{n/2} / \Gamma(\frac{n}{2} + 1)$ is the volume of an n -dimensional unit ball and $\Lambda_\nu(K, \eta)$, $\nu = 0, \dots, d-1$, are certain real coefficients that depend on K and η , but not on ϵ .

For eq. (14) to be true for all $\epsilon > 0$, it is crucial that K is convex [66]. Equation (14) is easily confirmed (and evaluated) for a convex polytope P . In this case, the set $(K \uplus B_\epsilon) \setminus P$ can be decomposed in an elementary way into wedges over the faces F of P as indicated by Fig. 4 (b1). Let $\mathcal{F}_\nu(P)$ denote the ν -dimensional faces of the polytope P § and

$$\mathbf{n}(P, F) := \{\mathbf{n}_P(\mathbf{x}) \in \mathbb{S}^{d-1} : \mathbf{p}_P(\mathbf{x}) \in \text{relint } F, \mathbf{x} \in \mathbb{R}^d \setminus P\} \quad (15)$$

§ \mathcal{F}_1 is the set of edges. In sec. 2 we use this notion for oriented edges, that is (non-oriented) edges are split into two oriented edges pointing in opposite directions. Here the set \mathcal{F}_1 contains non-oriented edges. Elsewhere it is stated explicitly.

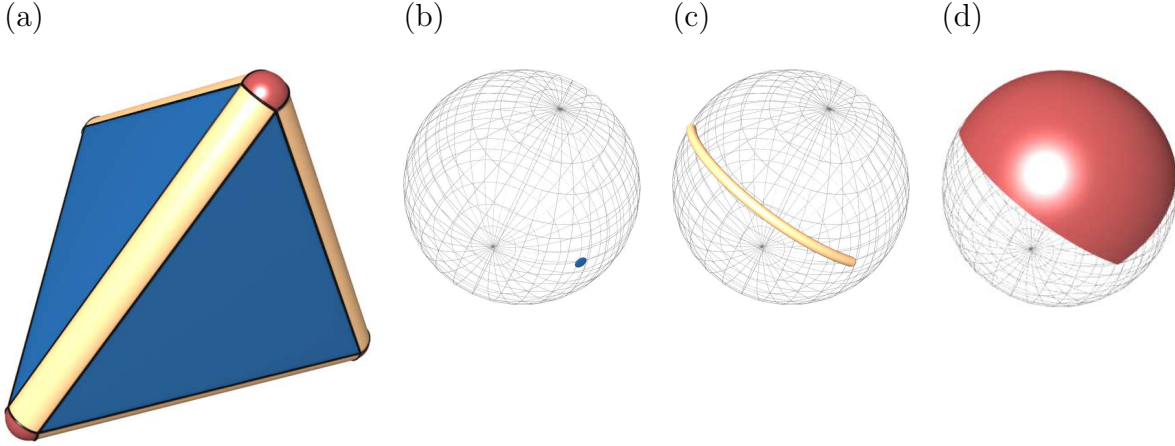


Figure 5. (a) Illustration of the set of normal vectors on the surface of a polytope P . (b) Normal vector assigned to a facet $F \in \mathcal{F}_2(P)$. (c) Line segment of normal vectors assigned to an edge $F \in \mathcal{F}_1(P)$. (d) Spherical triangle/patch of normal vectors assigned to a vertex $F \in \mathcal{F}_0(P)$.

the set of unit normal vectors assigned to $F \in \mathcal{F}_\nu(P)$ and relint F the relative interior of F (i.e. the interior of F w.r.t. the lowest-dimensional embedding affine hull); see Fig. 5. The contributions to $V_d(\mathcal{M}_\epsilon(K, \eta))$ coming from each of these wedges

$$\mathcal{M}_\epsilon(P, F) := \mathcal{M}_\epsilon(P, (\text{relint } F \times \mathbb{S}^{d-1})) \quad (16)$$

can be calculated by a simple integration known as Fubini's theorem or Cavalieri's principle [67, 68]. This shows that for $\eta = L \times S$ eq. (14) holds with

$$\Lambda_\nu(P, L \times S) = \frac{1}{\omega_{d-\nu}} \sum_{F \in \mathcal{F}_\nu(P)} \int_{F \cap L} d\mathcal{H}^\nu \int_{\mathbf{n}(P, F) \cap S} d\mathcal{H}^{d-\nu-1}, \quad (17)$$

where $\omega_\nu = \nu \kappa_\nu$ is the surface measure of the $(\nu - 1)$ -dimensional unit sphere and $d\mathcal{H}^\nu$ is the Hausdorff measure of dimension ν [69].

Since an arbitrary convex body K can be approximated by polytopes, eq. (14) can be derived by a continuity argument. In fact, $\Lambda_\nu(K, \eta)$ can be expressed as a linear combination of $V_d(\mathcal{M}_{\epsilon_\mu}(K, \eta))$, for $\epsilon_\mu > 0$ pairwise different and $\mu = 1, \dots, d$. One obtains an invertible $d \times d$ -matrix equation (with the matrix entries $\epsilon_\mu^{d-\nu} \kappa_{d-\nu}$) with ν running from $0, \dots, d - 1$. Therefore, the properties of the local parallel volume $V_d(\mathcal{M}_\epsilon(K, \eta))$ (in particular, additivity and weak continuity) are also available for $\Lambda_\nu(K, \eta)$ [64, p. 202]. In particular, $K \mapsto \Lambda_\nu(K, \eta)$ is an additive functional for fixed η . That is, for convex bodies K and K'

$$\Lambda_\nu(K \cup K', \eta) = \Lambda_\nu(K, \eta) + \Lambda_\nu(K', \eta) - \Lambda_\nu(K \cap K', \eta). \quad (18)$$

Furthermore, $\eta \mapsto \Lambda_\nu(K, \eta)$ is a non-negative measure for fixed K . The latter means that if $\eta_\mu \subset \mathbb{R}^d \times \mathbb{S}^{d-1}$, $\mu \in \mathbb{N}$, is a sequence of mutually disjoint (measurable) sets, then

$$\Lambda_\nu \left(K, \bigcup_{\mu=1}^{\infty} \eta_\mu \right) = \sum_{\mu=1}^{\infty} \Lambda_\nu(K, \eta_\mu). \quad (19)$$

This property is called σ -additivity of $\Lambda_\nu(K, \cdot)$. Weak continuity of Λ_ν means that for every sequence of convex bodies K_μ ($\mu \in \mathbb{N}$), with $K_\mu \rightarrow K$ and every continuous function $f : \mathbb{R}^d \times \mathbb{S}^{d-1} \rightarrow [0, \infty)$ the equation

$$\lim_{\mu \rightarrow \infty} \int f(\mathbf{x}, \mathbf{n}) \Lambda_\nu(K_\mu, d(\mathbf{x}, \mathbf{n})) = \int f(\mathbf{x}, \mathbf{n}) \Lambda_\nu(K, d(\mathbf{x}, \mathbf{n})) \quad (20)$$

holds. Note that this does not imply $\Lambda_\nu(K_\mu, \eta) \rightarrow \Lambda_\nu(K, \eta)$ as $\mu \rightarrow \infty$ for all measurable sets $\eta \subset \mathbb{R}^d \times \mathbb{S}^{d-1}$

In particular, $\Lambda_\nu(K, \cdot)$ can be used to integrate functions over $\mathbb{R}^d \times \mathbb{S}^{d-1}$. It is plausible that $\Lambda_\nu(K, \cdot)$ is concentrated on the normal bundle $N(K) := \{(\mathbf{p}_K(\mathbf{x}), \mathbf{n}_K(\mathbf{x})) \in \partial K \times \mathbb{S}^{d-1} : \mathbf{x} \in \mathbb{R}^d \setminus K\}$. In other words, $N(K)$ consists of all $(\mathbf{x}, \mathbf{n}) \in \partial K \times \mathbb{S}^{d-1}$ such that \mathbf{n} is an exterior unit normal vector of K at \mathbf{x} . The measures $\Lambda_\nu(K, \cdot)$, $\nu = 0, \dots, d-1$, are called *support measures* and are determined as coefficient measures of the Steiner formula, eq. (14). They are local versions of the classical MF W_ν , since $\Lambda_\nu(K, \mathbb{R}^d \times \mathbb{S}^{d-1}) = V_\nu(K) \propto W_{d-\nu}(K)$.

If K is sufficiently smooth, then

$$\Lambda_\nu(K, \eta) = \frac{\binom{d-1}{\nu}}{\omega_{d-\nu}} \int_{\partial K} \mathbf{1}\{(\mathbf{x}, \mathbf{n}_K(\mathbf{x})) \in \eta\} G_{d-\nu}(\mathbf{x}) dA, \quad (21)$$

where $G_\nu(\mathbf{x})$ is the $(\nu - 1)$ -th (normalised) elementary symmetric function of the principal curvatures of ∂K at \mathbf{x} . That is in three dimensions, these are 1, the mean curvature and Gaussian curvature, respectively. $\mathbf{1}\{\cdot\}$ is the characteristic function, which is evaluated to one if \cdot is true and 0 otherwise. For general dimensions and $\nu \leq d-1$, eq. (21) holds for all sufficiently smooth convex bodies K .

Having introduced the support measures as local versions of the scalar MF, it is easy to define the MT for a convex body K by

$$\Phi_\nu^{r,s}(K) := \frac{1}{r!s! \omega_{d-\nu+s}} \int_{\mathbb{R}^d \times \mathbb{S}^{d-1}} \mathbf{x}^r \mathbf{n}^s \Lambda_\nu(K, d(\mathbf{x}, \mathbf{n})), \quad (22)$$

hence we obtain $\Phi_\nu^{r,s}(K)$ by integrating the tensorial function $\mathbf{x}^r \mathbf{n}^s$ with respect to the measure $\Lambda_\nu(K, \cdot)$ over $N(K) \subset \mathbb{R}^d \times \mathbb{S}^{d-1}$. If K is a polytope, for $d = 3$ this yields equation (48), up to a different normalisation. If K is smooth, we obtain eq. (5), up to a different normalisation and indexing scheme, i.e.

$$\begin{aligned} \Phi_\nu^{r,s}(K) &= \frac{\binom{d-1}{\nu}}{r!s! \omega_{d-\nu+s}} \int_{\partial K} \mathbf{x}^r \mathbf{n}^s G_{d-\nu}(\mathbf{x}) dA, \\ \Phi_d^{r,0}(K) &= \frac{1}{r!} \int_K \mathbf{x}^r dV. \end{aligned} \quad (23)$$

The notation $\Phi_{\mu,r,s}$ or $\Phi_\mu^{r,s}$ for the MT in eq. (22) is preferred in some of the mathematical literature and differs from the notation $W_\nu^{r,s}$ in eqs. (4-5) only by a different indexing scheme and a different normalisation. In \mathbb{R}^3 , i.e. for $d = 3$, the functionals $\Phi_\mu^{r,s}$ and $W_\nu^{r,s}$ are related by

$$W_\nu^{r,s}(K) = C \Phi_{d-\nu}^{r,s}(K), \quad \text{with} \quad C := \frac{r!s! \omega_{\nu+s}}{d \binom{d-1}{\nu-1}}, \quad (24)$$

for $\nu = 1, \dots, d$, and

$$W_0^{r,0}(K) = r! \Phi_d^{r,0}(K). \quad (25)$$

The additivity and continuity properties of the support measures immediately yield the corresponding properties of the MT. This approach also shows that if it is possible to define support measures for a class of sets, then the corresponding tensor valuations can be defined by eq. (22).

Since the theory of support measures is well-developed [24, 64], the measure theoretic approach outlined above has some advantages over the differential geometric approach.

As a simple illustration, let us explain why $W_{d-\nu}^{1,1}$ is translation invariant for $\nu = 0, \dots, d-1$. Observe that by translation covariance of the support measures

$$\begin{aligned} & \int_{\mathbb{R}^d \times \mathbb{S}^{d-1}} \mathbf{x} \mathbf{n} \Lambda_\nu \left(K \uplus \mathbf{t}, d(\mathbf{x}, \mathbf{n}) \right) \\ &= \int_{\mathbb{R}^d \times \mathbb{S}^{d-1}} (\mathbf{x} + \mathbf{t}) \mathbf{n} \Lambda_\nu \left(K, d(\mathbf{x}, \mathbf{n}) \right) \\ &= \int_{\mathbb{R}^d \times \mathbb{S}^{d-1}} \mathbf{x} \mathbf{n} \Lambda_\nu \left(K, d(\mathbf{x}, \mathbf{n}) \right) + \mathbf{t} \int_{\mathbb{R}^d \times \mathbb{S}^{d-1}} \mathbf{n} \Lambda_\nu \left(K, d(\mathbf{x}, \mathbf{n}) \right). \end{aligned} \quad (26)$$

It is a basic property of the measures $\Lambda_\nu(K, \cdot)$ that they are centred at the origin in the sense that $\int \mathbf{n} \Lambda_\nu(K, d(\mathbf{x}, \mathbf{n})) = 0$ [35], which yields the assertion.

A natural and useful extension that is suggested by general measure theory is to introduce local tensor valuations by restricting the integration on the right-hand side of eq. (22) to measurable subsets of $\mathbb{R}^d \times \mathbb{S}^{d-1}$.

2. Bodies Bounded by Triangulated Surfaces

We describe an exact algorithm for all independent scalar, vectorial and rank-2 MT of bodies bounded by piece-wise linear (i.e. triangulated) surfaces. Henceforth such bodies, convex or non-convex, are called *polytopes* P and their bounding surface is the *triangulation* \mathcal{F} . Triangulations are commonly used as discrete approximations of smooth surfaces. The continuity of the MF and MT guarantee the convergence of the formula for the triangulations to the MF and MT of the smooth body.

The formulae are derived for convex bodies with triangulated bounding surfaces by considering parallel bodies P_ϵ of convex polytopes P (that is P_ϵ has a continuous normal fields and finite curvatures for $\epsilon > 0$ and a well defined limit as $\epsilon \rightarrow 0$). By application of the additivity relation these formulae are then shown to be valid also for bodies that are not convex. As the key results of this article—explicit formulae for the computation of MT of convex and non-convex polytopes—are summarised in table 2.

Consider a polytope P in \mathbb{R}^3 with piece-wise linear bounding surface $\partial P \equiv \mathcal{F}$. Without loss of generality the linear facets may be assumed to be triangles. The set of all triangular patches of ∂P is \mathcal{F}_2 , the set of oriented edges is \mathcal{F}_1 and the set of

|| It is an important consequence of the additivity relation that the MT (in contrast to e.g. the texture

vertices is \mathcal{F}_0 . We assume a *doubly connected edge list* (DCEL [70], also called *half edge data structure* [71]), that is, every edge which is shared between two triangles T and T' is a double-edge consisting of two oriented edges \mathbf{e} (being part of T) and \mathbf{e}' (part of T'), constituting an unambiguous assignment of each edge to a triangle. Each oriented edge is assigned to its previous edge $\mathbf{e}_{\text{previous}}$ and its next edge \mathbf{e}_{next} . The remaining ambiguity in the edge orientation is lifted by requiring the triangle normals $\mathbf{n}_T = (\mathbf{e}_{\text{previous}} \times \mathbf{e})/|\mathbf{e}_{\text{previous}} \times \mathbf{e}|$ to point out of the body P . Thus we can uniquely assign to each oriented edge \mathbf{e} a triangle T with vertices $\mathbf{v}_1, \mathbf{v}_2, \mathbf{v}_3$ (see Fig. 6) and its normal vector \mathbf{n}_T .

The parallel body construction is illustrated by Fig. 2 (b). For an arbitrary body P the parallel body P_ϵ with thickness $\epsilon > 0$ is defined as $P_\epsilon := P \uplus B_\epsilon$. For a convex polytope P (whose bounding surface has a discontinuous normal field) the bounding surface ∂P_ϵ has a continuous normal field. The curvatures are patch-wise constant: $G_2 = G_3 = 0$ on the planar patches, $G_2 = (2\epsilon)^{-1}$ and $G_3 = 0$ on the cylindrical patches corresponding to polygon edges, and $G_2 = 1/\epsilon$ and $G_3 = 1/\epsilon^2$ on the spherical patches corresponding to polytope vertices. For convex polytopes, the MT are defined as the surface integrals of eq. (5) evaluated on ∂P_ϵ in the limit $\epsilon \rightarrow 0$. The result thus obtained is equivalent with eq. (22), see also eq. (48).

2.1. Volume W_0

The calculation of the volume of a polytope P can be transformed into a surface integral by Gauss' law, see eq. (11) [72]. With $\text{div } \mathbf{x} = \text{div}(x, y, z)^t = 3$ one obtains

$$\begin{aligned} W_0(K) &= \int_P dV = \frac{1}{3} \int_P \text{div } \mathbf{x} dV = \frac{1}{3} \int_{\partial P} \langle \mathbf{x}, d\mathbf{A} \rangle \\ &= \text{tr} \frac{1}{3} \int_{\partial P} \mathbf{x} \mathbf{n} dA = \text{tr} W_1^{1,1} \end{aligned} \quad (27)$$

where $d\mathbf{A} = \mathbf{n} dA$ denotes the oriented infinitesimal area element and $\langle \cdot, \cdot \rangle$ the scalar product.

2.2. Surface area W_1 and integral mean curvature W_2

The surface integral is a sum over triangles and is easily evaluated yielding the formulae in Tab. 2. This result is independent whether P is convex or not. The surface area $W_1(P)$ of ∂P is simply the sum of triangle areas.

Expressing $W_2(P)$ as the limit of vanishing parallel distance ϵ of $W_2(P_\epsilon)$ of the parallel body P_ϵ , $W_2(P) = \lim_{\epsilon \rightarrow 0} W_2(P_\epsilon)$, the contributions of facets vanish because the mean curvature of a flat face is zero. The contribution of the spherical patches S corresponding to vertices vanishes because the integral over a spherical patch S can be parametrised in spherical coordinates by $\int \int_S \frac{1}{\epsilon} \epsilon^2 \sin \theta d\varphi d\theta$ which vanish as $\epsilon \rightarrow 0$.

tensor) do not change if flat polygonal facets are broken up into triangles. This is evidently also true for the algorithmic implementation described here.

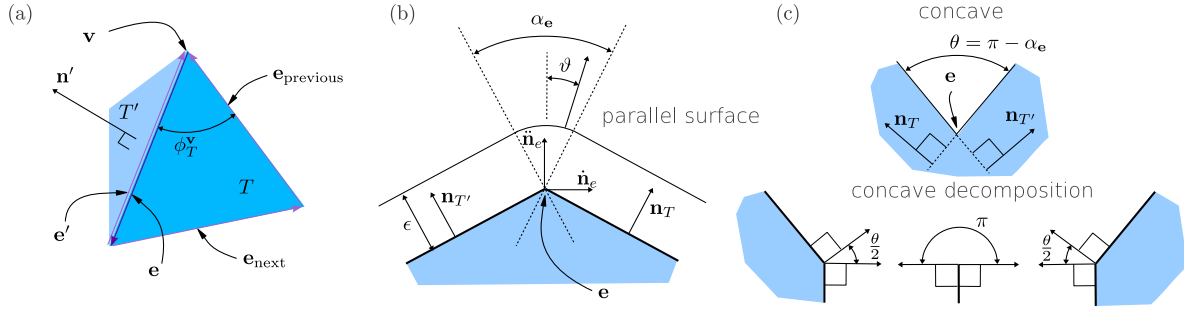


Figure 6. (a) Definition of geometric properties of a triangulated surface ∂P with doubly connected edge list (DCEL). Each edge \mathbf{e} is oriented and uniquely assigned to a triangle T . The counter oriented edge to \mathbf{e} is denoted \mathbf{e}' and assigned to the adjacent triangle T' . An oriented edge \mathbf{e} is unambiguously assigned to the previous edge $\mathbf{e}_{\text{previous}}$ and the next edge \mathbf{e}_{next} . The normal vector \mathbf{n}_T is defined to point out of the body K , i.e. $\mathbf{n}_T = (\mathbf{e}_{\text{previous}} \times \mathbf{e}) / |\mathbf{e}_{\text{previous}} \times \mathbf{e}|$. The angle between two edges of triangle T at vertex \mathbf{v} is denoted $\phi_T^{\mathbf{v}}$. (b) Cross-sectional view along an oriented edge \mathbf{e} . The normal vectors \mathbf{n}_T and $\mathbf{n}_{T'}$ of the triangle T (that contains \mathbf{e}) and T' span the angle $\alpha_{\mathbf{e}} \in (-\pi, \pi]$. A concave edge has a negative angle $\alpha_{\mathbf{e}}$. The figure also shows the definition of the local coordinate system used for the computation of $W_2^{0,2}$. The basis vectors $\hat{\mathbf{n}}_{\mathbf{e}}$, $\bar{\mathbf{n}}_{\mathbf{e}}$ and $\hat{\mathbf{e}}$ are defined as $\hat{\mathbf{e}} = \mathbf{e}/|\mathbf{e}|$, $\bar{\mathbf{n}}_{\mathbf{e}} = (\mathbf{n}_T + \mathbf{n}_{T'})/|\mathbf{n}_T + \mathbf{n}_{T'}|$ and $\hat{\mathbf{n}}_{\mathbf{e}} = \bar{\mathbf{n}}_{\mathbf{e}} \times \hat{\mathbf{e}}$. (c) Subdivision of a body P along a concave edge \mathbf{e} to yield locally convex bodies.

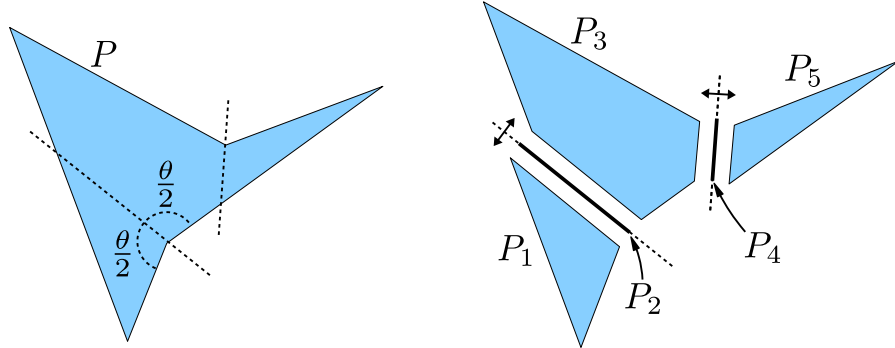


Figure 7. Subdivision of a non-convex body into convex sub-bodies, $P = P_1 \cup P_2 \cup P_3 \cup P_4 \cup P_5$. Note that for the computation of MT the segments P_2 and P_4 need to be taken into account, though their volume measure is 0: $W_0(P_2) = W_0(P_4) = 0$.

The remaining contribution of the edges is located at the cylindrical patches of ∂P_ϵ and is given in polar coordinates by

$$W_2(P) = \frac{1}{3} \lim_{\epsilon \rightarrow 0} \sum_{\mathbf{e} \in \mathcal{F}_1} \frac{1}{2} \int_0^{|\mathbf{e}|} dl \int_{-\alpha_{\mathbf{e}}/2}^{\alpha_{\mathbf{e}}/2} \frac{1}{2\epsilon} \epsilon d\vartheta = \sum_{\mathbf{e} \in \mathcal{F}_1} |\mathbf{e}| \frac{\alpha_{\mathbf{e}}}{12}, \quad (28)$$

where $|\mathbf{e}|$ is the length of edge \mathbf{e} and $\alpha_{\mathbf{e}}$ the dihedral angle, i.e. the angle between the surface normals of the two facets adjacent to \mathbf{e} . For a convex body, all edges have a dihedral angle $0 \leq \alpha_{\mathbf{e}} \leq \pi$; see also Fig. 6. Note that \mathcal{F}_1 is the set of oriented edges, i.e. the edge shared by two triangles is represented by two distinct oriented edges, which

scalar measures		
W_0	$\int_K dV$	$\frac{1}{3} \sum_{T \in \mathcal{F}_2} \langle \mathbf{C}_T, \mathbf{n}_T \rangle T $
W_1	$\frac{1}{3} \int_{\partial K} dA$	$\frac{1}{3} \sum_{T \in \mathcal{F}_2} T $
W_2	$\frac{1}{3} \int_{\partial K} G_2 dA$	$\frac{1}{12} \sum_{\mathbf{e} \in \mathcal{F}_1} \mathbf{e} \alpha_{\mathbf{e}}$
W_3	$\frac{1}{3} \int_{\partial K} G_3 dA$	$\frac{1}{3} \sum_{\mathbf{v} \in \mathcal{F}_0} (2\pi - \sum_{T \in \mathcal{F}_2(\mathbf{v})} \phi_T^{\mathbf{v}})$
vectorial measures		
$(W_0^{1,0})_i$	$\int_K \mathbf{x}_i dV$	$\sum_{T \in \mathcal{F}_2} (I_T)_{ik} (n_T)_k$, see sec. 2.4
$(W_1^{1,0})_i$	$\frac{1}{3} \int_{\partial K} \mathbf{x}_i dA$	$\frac{1}{3} \sum_{T \in \mathcal{F}_2} T (\mathbf{C}_T)_i$
$(W_2^{1,0})_i$	$\frac{1}{3} \int_{\partial K} G_2 \mathbf{x}_i dA$	$\frac{1}{12} \sum_{\mathbf{e} \in \mathcal{F}_1} \mathbf{e} \alpha_{\mathbf{e}} (\mathbf{C}_{\mathbf{e}})_i$
$(W_3^{1,0})_i$	$\frac{1}{3} \int_{\partial K} G_3 \mathbf{x}_i dA$	$\frac{1}{3} \sum_{\mathbf{v} \in \mathcal{F}_0} (2\pi - \sum_{T \in \mathcal{F}_2(\mathbf{v})} \phi_T^{\mathbf{v}}) \mathbf{v}_i$
tensorial measures (rank two)		
$(W_0^{2,0})_{ij}$	$\int_K \mathbf{x}_i \mathbf{x}_j dV$	$\sum_{T \in \mathcal{F}_2} (J_T)_{ijk} (n_T)_k$, see sec. 2.5
$(W_1^{2,0})_{ij}$	$\frac{1}{3} \int_{\partial K} \mathbf{x}_i \mathbf{x}_j dA$	$\frac{1}{3} \sum_{T \in \mathcal{F}_2} (I_T)_{ij}$
$(W_2^{2,0})_{ij}$	$\frac{1}{3} \int_{\partial K} G_2 \mathbf{x}_i \mathbf{x}_j dA$	$\frac{1}{36} \sum_{\mathbf{e} \in \mathcal{F}_1} \alpha_{\mathbf{e}} \mathbf{e} \cdot ((\mathbf{v}_1^2)_{ij} + (\mathbf{v}_1 \mathbf{v}_2)_{ij} + (\mathbf{v}_2^2)_{ij})$
$(W_3^{2,0})_{ij}$	$\frac{1}{3} \int_{\partial K} G_3 \mathbf{x}_i \mathbf{x}_j dA$	$\frac{1}{3} \sum_{\mathbf{v} \in \mathcal{F}_0} \left(2\pi - \sum_{T \in \mathcal{F}_2(\mathbf{v})} \phi_T^{\mathbf{v}} \right) (\mathbf{v}^2)_{ij}$
$(W_1^{0,2})_{ij}$	$\frac{1}{3} \int_{\partial K} \mathbf{n}_i \mathbf{n}_j dA$	$\frac{1}{3} \sum_{T \in \mathcal{F}_2} T (\mathbf{n}_T^2)_{ij}$
$(W_2^{0,2})_{ij}$	$\frac{1}{3} \int_{\partial K} G_2 \mathbf{n}_i \mathbf{n}_j dA$	$\frac{1}{24} \sum_{\mathbf{e} \in \mathcal{F}_1} \mathbf{e} ((\alpha_{\mathbf{e}} + \sin \alpha_{\mathbf{e}}) (\ddot{\mathbf{n}}_{\mathbf{e}}^2)_{ij} + (\alpha_{\mathbf{e}} - \sin \alpha_{\mathbf{e}}) (\dot{\mathbf{n}}_{\mathbf{e}}^2)_{ij})$

Second column: MF and MT for bodies with smooth boundary ∂K . The mean and Gaussian curvatures on ∂K are G_2 and G_3 , respectively. *Third column:* MF and MT for a triangulation. The set of facets of the triangulation \mathcal{F} is \mathcal{F}_2 , the set of oriented edges is \mathcal{F}_1 (in DCEL structure, see text) and the set of vertices \mathcal{F}_0 . The subset of triangles that contain the vertex \mathbf{v} is denoted by $\mathcal{F}_2(\mathbf{v})$. The nomenclature for triangulated surfaces is defined in Fig. 6. The vertices of an edge \mathbf{e} or a triangle T are denoted $\mathbf{v}_1, \mathbf{v}_2$ and \mathbf{v}_3 , respectively. $|T|$ is the area of $T \in \mathcal{F}_2$, \mathbf{C}_T its centre point $(\mathbf{v}_1 + \mathbf{v}_2 + \mathbf{v}_3)/3$ and the tensors I_T and J_T are given in eqs. (33) and (35) and table 3. $\mathbf{C}_{\mathbf{e}}$ is the centre point of edge \mathbf{e} , $\mathbf{C}_{\mathbf{e}} = (\mathbf{v}_1 + \mathbf{v}_2)/2$. $i, j, k \in \{x, y, z\}$, and $|e|$ its length. The symbol $\langle \cdot, \cdot \rangle$ denotes the scalar product. $\alpha_{\mathbf{e}}$ is the dihedral angle across edge \mathbf{e} , see sec. 2.2. \mathbf{n}_T is the normal of triangle T , pointing out of the body, see Fig. 6. The jump angles $\phi_T^{\mathbf{v}}$ are defined in sec. 2.3 and Fig. 8, and the quantities $\ddot{\mathbf{n}}_{\mathbf{e}}$ and $\dot{\mathbf{n}}_{\mathbf{e}}$ below eq. (37).

Table 2. MF and MT in 3D of body K with smooth boundary ∂K and a body P bounded by a triangulated surface ∂P .

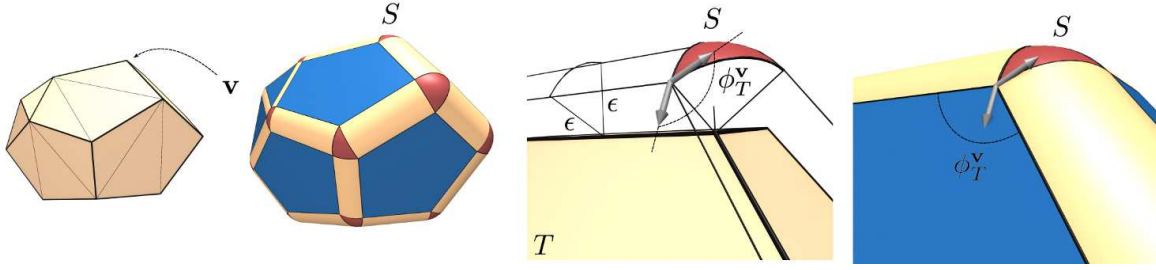


Figure 8. Sketch of a vertex \mathbf{v} with a spherical patch S of the parallel surface ∂P_ϵ . The interior angle in the triangle T adjacent to \mathbf{v} is denoted $\phi_T^{\mathbf{v}}$. S is a spherical polygon. The jump angles coincide with the interior angles of the triangles.

explains the factor $1/2$ in front of the integral.

Eq. (28) remains valid even if P is not convex, as is shown by exploiting additivity: A non-convex polytope P can be decomposed into a set of convex polytopes by cutting along the *symmetric bisector planes* of all concave edges (that is, $-\pi < \alpha_e < 0$), see Fig. 7. For a concave edge \mathbf{e} , the symmetric bisector plane is the plane that is spanned by \mathbf{e} and the average of the facet normals of the two facets adjacent to \mathbf{e} . By adding the contributions of all resulting convex bodies using the additivity relationship eq. (9), as outlined in Fig. 6 (c), one obtains the validity of eq. (28) for non-convex triangulated bodies. The sign of the dihedral angle $\alpha_e \in (-\pi, \pi]$ determines if the edge is convex ($\alpha_e > 0$) or concave ($\alpha_e < 0$).

2.3. Integral Gaussian curvature W_3 (Euler index χ)

As the point-wise Gaussian curvature G_3 on cylinders and flat facets vanishes, only vertices of the triangulation (and their corresponding spherical patches on the parallel body) contribute to W_3 . For both a convex and a non-convex polytope P the point-wise Gaussian curvature G_3 and the integrated Gaussian curvature W_3 can be calculated by the well-known simple sum over angle deficits at surface vertices in eq. (30), derived below, and also given in [73, 74]. The non-convex case is treated by exploiting additivity.

The Gaussian curvature contribution of the vertices $\mathbf{v} \in \mathcal{F}_0$ is derived by the Gauss-Bonnet-formula

$$\int_S G_3 dA = 2\pi - \sum_{T \in \mathcal{F}_2(\mathbf{v})} \phi_T^{\mathbf{v}} - \int_{\partial S} k_g ds, \quad (29)$$

where $\mathcal{F}_2(\mathbf{v})$ is the subset of triangles adjacent to vertex \mathbf{v} and S denotes the spherical patch on the parallel surface ∂P_ϵ . For all $\epsilon > 0$ each spherical cap $S \subset \partial P_\epsilon$ can be uniquely assigned to one vertex \mathbf{v} ; ∂S its oriented boundary curve and k_g the geodesic curvature along ∂S . At the corners of ∂S , the discontinuity of the tangent vectors is

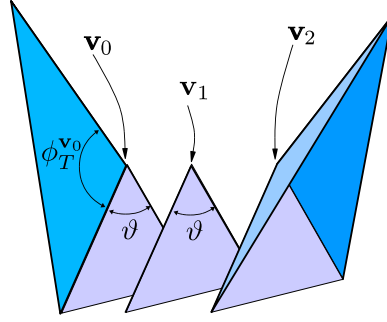


Figure 9. The Gaussian curvature G_3 at a saddle vertex is obtained by a virtual decomposition of P at \mathbf{v} into three polytopes with vertices \mathbf{v}_μ , $\mu = 1, 2, 3$ using the additivity property of MT.

characterised by *jump angles* $\phi_T^{\mathbf{v}}$ (see Fig. 8) which for all $\epsilon > 0$ coincide with the interior angles of the triangle T at \mathbf{v} [75], see Fig. 8. The geodesic curvature k_g vanishes almost everywhere along ∂S , because ∂S are great circle arcs on the spherical patch and the adjacent cylindrical patch and are thus geodesics; hence the integral $\int_{\partial S} k_g ds$ vanishes.

As a consequence, $\int_S G_3 dA$ is constant for all $\epsilon > 0$. Equation (29) therefore yields a definition and an explicit formula for $W_3(P)$ as a sum of the local contribution $w_3(P, \mathbf{v})$ at a vertex \mathbf{v}

$$W_3(P) = \frac{1}{3} \sum_{\mathbf{v} \in \mathcal{F}_0} w_3(P, \mathbf{v}) = \frac{1}{3} \sum_{\mathbf{v} \in \mathcal{F}_0} \left(2\pi - \sum_{T \in \mathcal{F}_2(\mathbf{v})} \phi_T^{\mathbf{v}} \right). \quad (30)$$

At a concave vertex \mathbf{v} , a polytope P can always be decomposed into three separate bodies (one of vanishing volume) that have convex vertices in lieu of \mathbf{v} . It is easy to validate eq. (30) at concave vertices by using the additivity relation in eq. (9), see Fig. 9.

2.4. Centre of mass $W_0^{1,0}/W_0$ and curvature centroids $W_\nu^{1,0}/W_\nu$

The Minkowski vector $W_0^{1,0}$ corresponds to the centre of mass of P multiplied with its volume (assuming P is homogeneously filled with material of constant density.) The components of this vector may be computed by transforming the volume integral into a surface integral using Gauss' theorem

$$(W_0^{1,0}(P))_i = \int_P \mathbf{x}_i dV = \int_{\partial P} \langle \mathbf{f}_i, d\mathbf{A} \rangle \quad (31)$$

with functions \mathbf{f}_i that satisfy $\text{div} \mathbf{f}_i = \mathbf{x}_i$. The vector-valued auxiliary function \mathbf{f}_i can be chosen for each index i independently and the index i denotes the index of $W_0^{1,0}$, which is evaluated. For the particular choice of \mathbf{f}_i given in table 3, this can be explicitly written as

$$(W_0^{1,0}(K))_i = \sum_{T \in \mathcal{F}_2} \int_T \mathbf{x}_i \mathbf{x}_k (\mathbf{n}_T)_k dA = \sum_{T \in \mathcal{F}_2} (I_T)_{ik} (\mathbf{n}_T)_k \quad (32)$$

$W_0^{1,0}$			$W_0^{2,0}$		
i	\mathbf{f}_i	k	i, j	\mathbf{f}_{ij}	k
x	$(0, xy, 0)^t$	y	x, x	$(0, 0, xxz)^t$	z
y	$(0, 0, yz)^t$	z	y, y	$(0, 0, yyz)^t$	z
z	$(xz, 0, 0)^t$	x	z, z	$(0, zz y, 0)^t$	y
			x, y	$(0, 0, xyz)^t$	z
			x, z	$(0, xyz, 0)^t$	y
			y, z	$(xyz, 0, 0)^t$	x

Table 3. Auxiliary functions used to convert the volume integrals of $W_0^{1,0}$ and $W_0^{2,0}$ into surface integrals.

with k as listed in table 3. (k is not a summation index.) $|T|$ is the surface area of T . The I_T in eq. (32) are tensorial integrals over the individually parametrised triangles with the three vertices \mathbf{v}_μ , $\mu = 1, 2, 3$

$$I_T = 2|T| \int_0^1 da \int_0^{1-a} db [\mathbf{v}_1 + a(\mathbf{v}_2 - \mathbf{v}_1) + b(\mathbf{v}_3 - \mathbf{v}_1)]^2. \quad (33)$$

The components of the auxiliary functions $(\mathbf{f}_i)_k$ are selected entries of the tensor I_T or zero. I_T can be written in terms of the triangle vertices \mathbf{v}_μ and triangle centres \mathbf{C}_T of T as

$$I_T = 2|T| \left(\frac{9}{24} \mathbf{C}_T^2 + \frac{1}{24} \sum_{\mu=1}^3 \mathbf{v}_\mu^2 \right). \quad (34)$$

The remaining integrals $W_\nu^{1,0}$ with $\nu = 1, 2, 3$ are evaluated similarly to the integrals W_ν , $W_\nu^{2,0}$ (see below). The integrals $W_\nu^{0,1}$ ($\nu = 1, 2, 3$) involving surface normals vanish for arbitrary bodies (with closed bounding surfaces).

2.5. Volume integral $W_0^{2,0}$

The volume integral $W_0^{2,0}(P)$ can be computed in a similar way as $W_0^{1,0}(P)$. Using

$$J_T = 2|T| \int_0^1 da \int_0^{1-a} db [\mathbf{v}_1 + a(\mathbf{v}_2 - \mathbf{v}_1) + b(\mathbf{v}_3 - \mathbf{v}_1)]^3, \quad (35)$$

the components ij of the tensor may be expressed as

$$(W_0^{2,0}(K))_{ij} = \sum_{T \in \mathcal{F}_2} (J_T)_{ijk} (\mathbf{n}_T)_k. \quad (36)$$

Again, the index k is not a summation index but rather the index specified in table 3. This derivation applies equally to convex and non-convex polytopes P .

2.6. Surface integrals $W_1^{0,2}$ and $W_2^{0,2}$

The computation of $W_1^{0,2}$ results in a simple sum of integrals over triangular facets, resulting in the formulae in Tab. 2, both for convex and non-convex bodies.

The tensor $W_2^{0,2}$ is calculated by a parallel body construction, first demonstrated for convex bodies. Consider a convex polytope P , and the corresponding parallel body P_ϵ . The integral over the parallel surface is split up into integrals over flat facets, cylindrical patches and spherical patches. Out of these only the cylindrical edge segments contribute, for the same reasons as for the scalar measure W_2 . The remaining contribution is calculated for $\epsilon \rightarrow 0$ using the following representation for the normal vectors on the cylindrical patches. Given an edge \mathbf{e} with facet normals \mathbf{n}_T and $\mathbf{n}_{T'}$ of the adjacent triangles. One obtains, also representing a special case of eq. (48),

$$W_2^{0,2}(K) = \frac{1}{12} \sum_{\mathbf{e} \in \mathcal{F}_1} |\mathbf{e}| \int_{-\alpha_{\mathbf{e}}/2}^{\alpha_{\mathbf{e}}/2} \mathbf{n}^2 d\vartheta. \quad (37)$$

To compute the integral on the right hand side we define the orthogonal unit vectors $\hat{\mathbf{e}} = \mathbf{e}/|\mathbf{e}|$, $\hat{\mathbf{n}} = (\mathbf{n}_{\mathbf{e}_T} + \mathbf{n}_{\mathbf{e}_{T'}})/|\mathbf{n}_{\mathbf{e}_T} + \mathbf{n}_{\mathbf{e}_{T'}}|$ and $\hat{\mathbf{n}} = \hat{\mathbf{e}} \times \hat{\mathbf{n}}$. For a given edge, $\mathbf{n}(\vartheta)$ can be written as $\mathbf{n} = \cos \vartheta \hat{\mathbf{n}} + \sin \vartheta \hat{\mathbf{n}}$. In this basis, the integral over \mathbf{n}^2 evaluates to $(1/2) ((\alpha_{\mathbf{e}} + \sin \alpha_{\mathbf{e}}) \hat{\mathbf{n}}^2 + (\alpha_{\mathbf{e}} - \sin \alpha_{\mathbf{e}}) \hat{\mathbf{n}}^2)$, see Fig. 6. This yields the formula in Tab. 2. The validity of this formula for non-convex bodies follows from the same additivity arguments as for W_2 .

2.7. Curvature-weighted surface integrals $W_2^{2,0}$ and $W_3^{2,0}$

The mean and Gaussian curvature weighted surface integrals $W_2^{2,0}$ and $W_3^{2,0}$ over position vectors can be evaluated as the limit $\epsilon \rightarrow 0$ of the parallel body construction, for convex bodies. The validity for non-convex shapes follows from the analogous construction as for W_2 and W_3 (see tab. 2).

2.8. Open bodies, labelled domains and Minkowski maps

The analysis presented so far has been derived for compact bodies in \mathbb{R}^3 with a *closed* bounding surface – and inherits strong robustness from its integral nature. For some analyses, the requirement of closed bodies is too stringent. For example, experimental data sets of percolating or periodic structures, both of which extend infinitely through space, always represent finite subsets of the structure with components that traverse the data set boundaries. Similarly, an analysis of a periodic model may be restricted to a translational unit cell, see Fig. 10. Furthermore, a *local* MT analysis, termed a *Minkowski map* [16, 6], can be useful to quantify variations throughout the sample. For a Minkowski map, a grid is superposed on the body K , and the MT are computed separately for each grid domain L . Such Minkowski maps can be useful to analyse

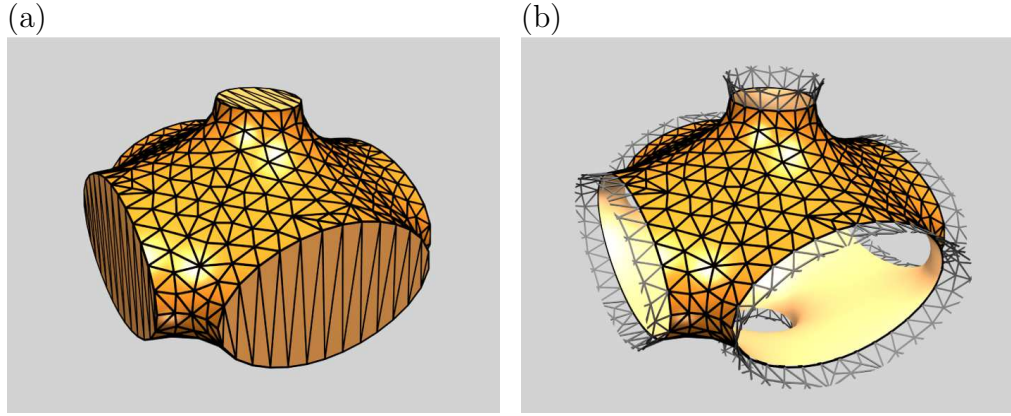


Figure 10. (a) A compact (but not convex) body K that corresponds to a translational unit cell of a periodic body and a triangulation of it. Its bounding surface consists in the translational unit as well as the flat “end caps” that seal it. (b) A surface portion representing a translational unit and its triangulation. The body K is the volume to one side of the surface and forms a connected periodic body. The surface and its triangulation extend beyond the translational unit cell indicating that the surface (and the triangulation) is periodic.

spatial heterogeneity of anisotropy or orientation at the length scale given by the size of L . In these situations, the MT are computed for the subset $L \cap \partial K$ of the whole bounding surface that is contained in a box L . In general, $L \cap \partial K$ is not a closed surface even if ∂K is.

It is evidently possible to take the subset $K \cap L$ of K and consider $\partial(K \cap L)$ as the bounding surface. However this introduces bounding surface patches (e.g. solid/void interfaces if K is a porous medium) that are not part of the bounding surface ∂K of K . For physical analyses one may want to avoid such *boundary effects*, i.e. not consider the contributions of these additional bounding surface patches. This motivates the introduction of MF and MT for open bodies, i.e. bodies without a closed bounding surface (see Fig. 10).

In lieu of an attempt to define MF and MT for open bodies, we define a domain-wise analysis of MF and MT. Consider a decomposition of the surface ∂P of a triangulated body P into m domains, or patches, D_σ (with $\sigma = 1, \dots, m$) such that

$$\partial P = \bigcup_{\sigma=1}^m D_\sigma, \quad (38)$$

and consider these domains *label ed* by labels $\sigma = 1, \dots, m$. Triangles are uniquely assigned to a label, but edges and vertices of the triangulation can be shared between several domains. Specifically, the domains D_σ could represent a decomposition of P into patches contained within the grid domains of a three-dimensional lattice (See Fig. 11).

Contributions of the facets can be uniquely assigned to D_σ , but the contribution of edges and vertices on the boundaries of a patch D_σ needs to be divided between σ and the label of the adjacent domain σ' (See Fig. 11).

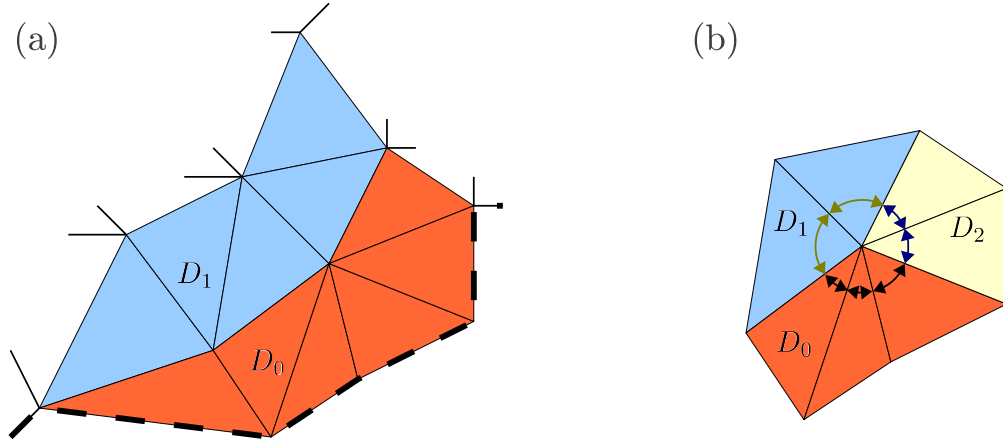


Figure 11. (a) A triangulated surface may be decomposed into several domains by assigning a domain label to each triangle; also open boundaries are possible, i.e. triangle edges without adjacent triangles (thick dashed line). (b) Label factors at vertices which are adjacent to triangles of more than one domain. The Gaussian curvature contribution is weighted with the interior angles belonging to each domain.

For $W_2^{r,s}$, the contribution of the dihedral angle at an edge is equally divided between the labels of the two adjacent triangles (Note that this is naturally taken account of by the use of oriented edges in the doubly-connected edge list, discussed above). For $W_3^{r,s}$ the division of the contribution of the interior vertex angles to the integral Gaussian curvature measures $W_3^{r,s}$ is less straight-forward. An intuitive way, that is also consistent with global integration over all labelled domains, is provided by the use of *label factors*. The label factor $f_{D_\sigma}(\mathbf{v})$ of domain D_σ at vertex \mathbf{v} is defined as

$$f_{D_\sigma}(\mathbf{v}) := \frac{\sum_{T \in \mathcal{F}_2(\mathbf{v}) \cap \mathcal{F}_2(D_\sigma)} \phi_T^{\mathbf{v}}}{\sum_{T \in \mathcal{F}_2(\mathbf{v})} \phi_T^{\mathbf{v}}}, \quad (39)$$

where $\mathcal{F}_2(D_\sigma)$ is the set of all triangles labelled with label σ . Hence $f_{D_\sigma}(\mathbf{v})$ is the sum of angles at \mathbf{v} of those triangles adjacent to \mathbf{v} and are labelled σ divided by sum of these angles of all adjacent triangles. It is easy to see, that

$$w_3(\mathbf{v}) = \sum_{\sigma=0}^m f_{D_\sigma}(\mathbf{v}) w_3(\mathbf{v}), \quad (40)$$

for a vertex with m adjacent labels and $W_3(P) = \sum_{\mathbf{v} \in \mathcal{F}_0} w_3(\mathbf{v})$.

For the volume tensor $W_0^{2,0}$ a label-wise analysis is only well-defined if the body K is subdivided (and not only the bounding surface ∂K).

2.9. Implementation details and “karambola” software package

A fully functional implementation of the algorithms represented in sections 2.1 to 2.8 is provided as online supplementary material to this article, and also made available

through the internet at www.theorie1.physik.fau.de/karambola, under a GNU General Public License.

The implementation is a straightforward realisation of the formulae in the rightmost column of Tab. 2 into ANSI-C code. A simple data structure is used to store a triangulation of a surface, as a set of points and a list of facets (specifically triangles); the data structure allows to iterate over all vertices, edges or facets by simple loops, for example over all edges “for e in \mathcal{F}_1 ”, and it allows the extraction of neighbours, for example of all (one or two) triangles that are adjacent to a given edge e . With that data structure in place, the sums in Tab. 2 simply become for loops, that are all linear in the number of edges, facets or vertices.

3. Anisotropy Measures

Based on MT, robust measures of anisotropy can be defined that are sufficiently sensitive to capture subtle anisotropy effects and that are applicable to a wide range of microstructures. The usefulness and versatility of this approach is demonstrated by two examples representing different types of structures – a cellular partition and a network structure.

A rank-2 tensor is defined to be *isotropic* if and only if it is proportional to the unit tensor Q , i.e. its eigenvalues are all equal. Deviations from isotropy are measured by the anisotropy index $\beta_\nu^{r,s}$, which is the ratio of extremal eigenvalues of the tensor $W_\nu^{r,s}$. For example, let ξ_μ ($|\xi_1| \leq |\xi_2| \leq |\xi_3|$) be the eigenvalues of $W_1^{0,2}$, then the anisotropy index is

$$\beta_1^{0,2} := \left| \frac{\xi_1}{\xi_3} \right| \in [0, 1]. \quad (41)$$

By definition, this quantity is dimensionless, continuous and rotation invariant. The value of 1 indicates perfect isotropy, and smaller values indicate anisotropy. For anisotropic bodies, it is sometimes also useful to consider $\gamma_1^{0,2} = |\xi_2/\xi_3|$.

These quantities can be easily interpreted for the translation invariant tensors $W_1^{0,2}$ and $W_2^{0,2}$. We can write $W_1^{0,2}$ equivalently to eq. (22) as the second moment of the distribution of normal vectors (with the density $\rho_1(\mathbf{n})$) on the unit sphere \mathbb{S}^2 as

$$W_1^{0,2}(K) = \frac{1}{3} \int_{\mathbb{S}^2} \rho_1(\mathbf{n}) \mathbf{n} \odot \mathbf{n} \, d\Omega, \quad (42)$$

where the $\rho_1(\mathbf{n}') = \int_{\partial K} \delta(\mathbf{n} - \mathbf{n}') \, dA$. That is, ρ_1 is area-weighted density of normal vectors. It is easy to see that an uniform distribution on \mathbb{S}^2 is equivalent to an isotropic tensor.

For example, if K is a sphere, then $\rho_1(\mathbf{n})$ is constant and $\beta_1^{0,2} = 1$ as expected. For the rectangular box $[0, a_x] \times [0, a_y] \times [0, a_z]$, the function $\rho_1(\mathbf{n})$ is concentrated at delta peaks,

$$\rho_1(\mathbf{n}) = a_x a_y a_z \sum_{i=x,y,z} \frac{\delta(\mathbf{e}_i - \mathbf{n}) + \delta(\mathbf{e}_i + \mathbf{n})}{a_i} \quad (43)$$

The resulting anisotropy measure is a_z/a_x for $a_x \geq a_y \geq a_z$.

It is instructive to express the second translation-invariant MT $W_2^{0,2}$ by a distribution of normals and curvatures. The density

$$\rho_2(\mathbf{n}', G_2') = \int_{\partial K} \delta(\mathbf{n} - \mathbf{n}') \delta(G_2 - G_2') dA \quad (44)$$

gives the sum of the area of all surface patches that have normal direction \mathbf{n}' and mean curvature G_2' .

$$W_2^{0,2}(K) = \frac{1}{3} \int_{-\infty}^{\infty} G_2 \int_{\mathbb{S}^2} \rho_2(\mathbf{n}, G_2) \mathbf{n} \odot \mathbf{n} d\Omega dG_2. \quad (45)$$

If the function ρ_2 can be written as a product $\rho_2(\mathbf{n}, G_2) = \tilde{\rho}_2(G_2) \rho_1(\mathbf{n})$, the anisotropy characteristics $\beta_1^{0,2}$ and $\beta_2^{0,2}$ defined as the ratio of the smallest to the largest eigenvalue of $W_2^{0,2}$ are identical. In this sense, $\beta_2^{0,2}$ provides a higher order anisotropy measure that quantifies anisotropy of the curvature distribution.

3.1. Alignment of Actin Biopolymer networks under shear

Biopolymer networks made of actin or collagen fibres are important structural elements in biological tissue that act as a scaffolds and provide stiffness and mechanical stability [77, 78, 79]. Of current interest is the relationship between fibre arrangement and alignment on the one hand side and elastic or visco-elastic properties on the other. This relationship can be probed by shear-experiments with confocal microscopy providing real-space structural data [76]. We now demonstrate that the degree of alignment and of structural anisotropy of the fibre network is well-captured by a MT analysis.

The data sets analysed here represent Actin fibre networks reconstituted from rabbit actin biopolymer networks with actin concentration of 1.2mg/ml cross-linked with filamin A. These are imaged using confocal microscopy for different shear deformations, see the explanation in Fig. 12. The data sets are the same as those analysed in [76]. The gray-scale data set is converted into a binary data set with 1 corresponding to actin and 0 corresponding to the surrounding fluid by standard threshold segmentation with threshold I_c ¶. The medial axis of the 1 phase is computed using distance-ordered homotopic thinning [80, 81] and is used as the one-voxel thick line representation of the actin fibre network. Conversion to a triangulated representation is obtained by using the Marching Cubes algorithm [82]. For more details of the analysis of biopolymers see ref. [83].

¶ The threshold I_c is chosen such that only the brightest and hence thickest fibres are retained. For a given segmentation threshold I_c the integrated intensity of all voxels of the fluid phase is $\Lambda = (\sum I(p))^{-1} \sum^* I(p)$ where $I(p)$ is the intensity of voxel p in the original intensity data set, \sum the sum over all voxels of the data set and \sum^* the sum over all voxels of the fluid phase, i.e. those voxels that are set to 0 by the segmentation process. The values of I_c chosen here correspond to $0.95 < \Lambda < 0.99$.

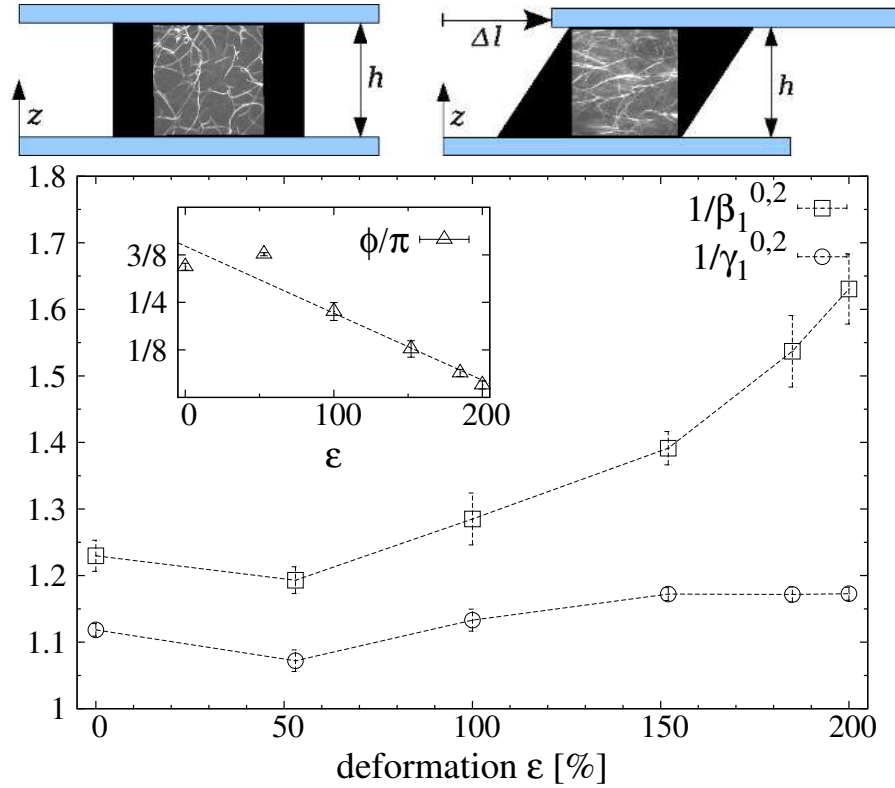


Figure 12. Anisotropy measures $1/\beta_1^{0,2}$ and $1/\gamma_1^{0,2}$ of actin network as function of shear. The ratio of largest to the smallest eigenvalue $1/\beta_1^{0,2}$ grows with increasing shear indicating that the fibers become increasingly aligned. The ratio of the largest to the intermediate eigenvalue $1/\gamma_1^{0,2}$ remains close to unity as expected since the fibres are essentially one-dimensional lines, inflated to approximately cylindrical tubes. The insert shows the alignment angle ϕ of the eigenvector corresponding to the minimal eigenvalue ξ_1 of $W_1^{0,2}$ and the direction of applied shear; its decay to 0 indicates that the network aligns with the shear direction when large shear is applied. The error bars in both plots are the standard deviation of the distribution of the quantities when analysed for different segmentation parameter between $0.95 < \Lambda < 0.99$. The illustrations above sketch the experimental setup with confocal microscopy images corresponding to a fibre network at shear $\epsilon := \Delta l/h = 0$ and $\epsilon = 2$ (the small confocal microscopy images are taken from [76]).

Typically only a subset, or observation window, of the structure is available for analysis. Therefore we assume that the network is homogeneous and a sufficiently large but finite subset is accessible which is assumed to represent the entire sample. The derived measures $\beta_1^{0,2}$ quantify the intrinsic anisotropy, i.e. their values do not depend on the size, aspect ratio or position of the observation window (for sufficiently large windows).

Figure 12 shows $1/\beta_1^{0,2}$ and $1/\gamma_1^{0,2}$ evaluated on the whole network (that consists essentially in a single component; only the outer boundary layers of the confocal data are clipped). It shows that the distribution of normal directions of the fibre bounding surface becomes less isotropic with increasing shear, indicating alignment

of the fibres. The angle between the eigenvector to the minimal eigenvalue ξ_1 (corresponding approximately to the dominant tangent direction) and the direction of shear decreases to 0, indicating the alignment of the fibres with the direction of shear. This is commensurate with the results published in [76], that extracted a distribution of tangent directions and used these to quantify alignment.

The eigenvalue ratios of the translation-covariant tensors $W_\nu^{2,0}$ (and of the tensor of inertia) capture different aspects of the anisotropy of a shape compared to the translation invariant tensors $W_\nu^{0,2}$, see also section 1.1. However, usefulness of the translation-covariant tensors depends on whether or not a natural definition of the origin is available for the system. For example, for the analysis of cellular shapes one may choose the centre of mass $W_0^{1,0}/W_0$ or the corresponding curvature centroid $W_\nu^{1,0}/W_\nu$ as the origin. Especially for percolating or periodic bodies, for which the analysis is always restricted to a finite window of observation, the choice of origin is often not naturally determined. An additional problem for such structures is that the measures $\beta_\nu^{2,0}$ derived from translation covariant tensors $W_\nu^{2,0}$, as opposed to the translation-invariant measures $\beta_\nu^{0,2}$, crucially depend on the shape and size of the window of observation.

The analysis of alignment of biopolymer networks illustrates the potential of the MT approach for structure characterisation of cellular and porous materials, and demonstrates its applicability to voxelised experimental data. The MT approach can shed light on systems with a similar spatial structure that exhibit subtle anisotropy effects, such as fibrous biological materials [84], porous materials[4], and metal foams [85].

3.2. Anisotropy of free-volume cells of random bead Packs

Granular media represent a system where geometry plays an essential role in determining its physical properties, such as flow or packing properties. The geometric structure to be characterised is substantially different from the above example. It consists in an assembly of (disjoint) grains that have, at most, mutual point contacts.

A commonly used way to associate each grain with *its* corresponding region of space is the construction of a Voronoi diagram. The distributions of volumes of the Voronoi cells of disordered jammed sphere packs with packing fractions from 0.55 (random loose packing) to around 0.64 (random close packing, RCP) have attracted interest for the study of granular systems [86], motivated by a possible statistical mechanics description of granular systems [87, 88]. For instance, Aste *et al.* [86] used the volume distribution of Voronoi cells to estimate configurational entropy in static packings, and Zhao *et al.* [89] to quantify spatial correlations in disc packings.

Here we illustrate how Minkowski tensors can be used to characterise the shape, rather than simply the volume, of the grains' Voronoi cells, in the spirit of reference [1].

Figure 13 shows a subset of an experimental data set of static disordered monodisperse jammed spheres with packing fraction 0.58 on the left panel (details see

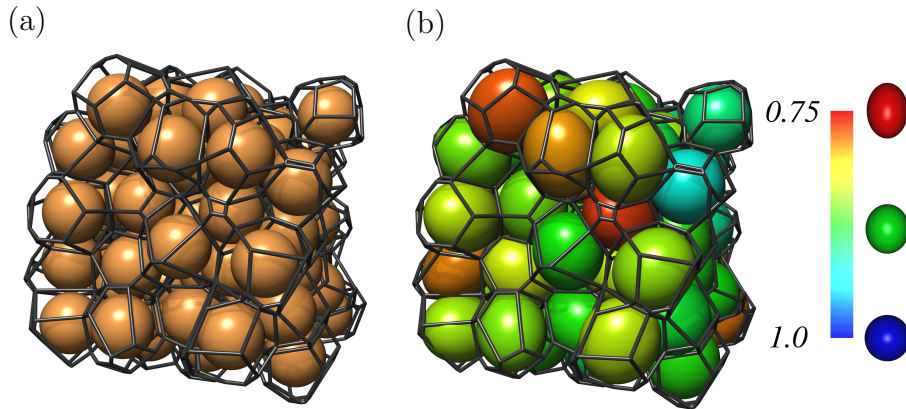


Figure 13. (a) Voronoi diagram of jammed monodisperse sphere pack. (b) The same Voronoi diagram, but spheres are replaced by ellipsoids with half-axes $a_1 = a_2 < a_3$, aligned along the eigendirections of $W_0^{2,0}$. Colours represent the ratio of the shortest and longest axis of the ellipsoid. See also Fig. 15 in the appendix for the relation of the half axes ratios a_1/a_3 to the MT anisotropy measure $\beta_0^{2,0}$ for ellipsoidal particles. (figure reproduced from ref. [1]).

ref. [1]) The wire-frame illustrates the Voronoi diagram of these spheres⁺. On the right hand side, spheres were replaced by ellipsoids that have the same eigenvalue ratio of the Minkowski tensor $W_0^{2,0}$ as their Voronoi cells, $W_0^{2,0}(\text{ellipsoid}) = W_0^{2,0}(\text{Voronoi cell})$, implying in particular the same value of the anisotropy measure $\beta_0^{2,0}$. Their half-axes are aligned with the eigendirections of the tensor $W_0^{2,0}$, evaluated for the corresponding Voronoi cell. The use of MT, and their eigenvalues and eigendirections, hence provides an efficient way of ‘fitting’ ellipsoids to given convex cells and hence a means to quantify their anisotropy or elongation. This in turn provides sensitive tools to quantify shape and structure of both amorphous and ordered particulate systems and packings.

Quantitative analyses of the Voronoi cell shapes of disordered sphere configurations, in various phases, have been given in references [1, 7, 2, 92], illustrating the breadth of the Minkowski tensor approach and in particular its usefulness to capture the onset of crystallisation. An application to ordered sphere packings has been given in preliminary form in the conference proceeding [93].

The scope of Minkowski tensors for the analysis of granular material is however not restricted to the detection of local crystalline domains. Rather, as the following analysis illustrates, these shape measures also allow for a quantitative description of the local structure in *amorphous* assemblies, discriminating sharply between different types of amorphous geometries.

Figure 14 shows a study where the simple anisotropy measure $\beta_0^{2,0}$ derived from the Minkowski tensors reveals a distinct difference between the different phases that hard sphere systems can adopt: the plot shows the typical shape, quantified by

⁺ The Voronoi cells of the sphere centres are computed using the program *qhull* [90]. For a point \mathbf{p} of a set \mathcal{P} of points, its Voronoi cell is the convex polytope that contains all points of \mathbb{R}^3 closer to \mathbf{p} than to any other point in \mathcal{P} [91].

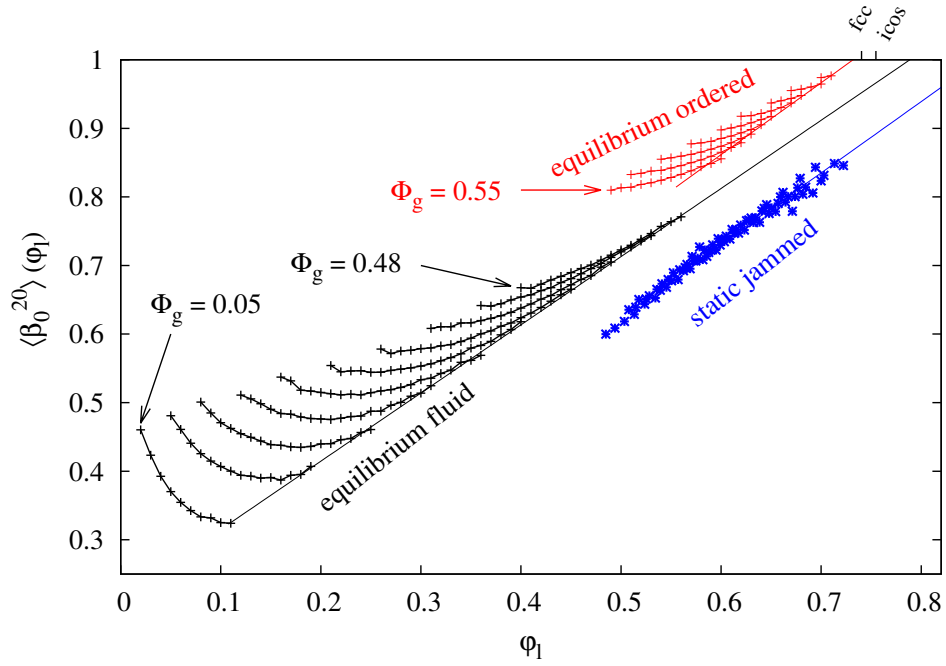


Figure 14. Voronoi cell anisotropies quantified by $\beta_0^{2,0}$ as function of local packing fraction ϕ_l , for equilibrium hard spheres in the fluid phase and in the ordered phase and for jammed static disordered sphere packs. The data representing static jammed spheres represent 6 distinct sphere configurations (including tomographic images and simulations with and without friction and gravity [94, 95, 96]) each with a different global packing fraction $0.585 \leq \phi_g \leq 0.64$; these are the same used in Fig. 6 of [1]. The equilibrium hard sphere data is obtained from Monte Carlo simulations, and comprise 4000 to 16000 spheres, see ref. [2] for details. “fcc” marks the packing fraction of the densest crystallographic sphere pack $\phi_g = \phi_l = \pi/\sqrt{18} \approx 0.7404$ and “ico” the densest possible local configuration $\phi_{\text{ico}} = (25 + 11\sqrt{5})^{3/2}\pi/[15\sqrt{10}(15 + 7\sqrt{5})] \approx 0.7547$. The straight lines represent guides-to-the-eye only for what may be the common asymptotic behaviour of the sets of curves of each phase. Note in particular that the data for static jammed spheres appears to collapse to a single curve, independent on global packing fraction and packing protocol, in contrast to the equilibrium systems. (A script to generate this plot is added as online supplementary material, in the `demo` subfolder of the `karambola` Minkowski tensor program.)

$\beta_0^{2,0}$, of a Voronoi cell of a given volume, expressed as the local packing fraction $\phi_l := W_1(\text{grain})/W_1(\text{Voronoi cell})$. The plot contains data for equilibrium hard sphere systems in the fluid and in the ordered phase (the same data as used in reference [2]) and of jammed static sphere packs (the same data sets mentioned above and used in Fig. 6 of ref. [1]). For each sphere configuration, the Voronoi cells of all particles are computed and their *local packing fractions* ϕ_l . Then all cells are classified by their value of ϕ_l , and the average cell shape $\langle \beta_0^{2,0} \rangle(\phi_l)$ is determined by averaging $\beta_0^{2,0}$ over all cells of a data set that have, up to a discretisation interval $\Delta\phi_l$, the same value of ϕ_l . The curves $\langle \beta_0^{2,0} \rangle(\phi_l)$ describe Voronoi cell anisotropy as function of the local packing fraction ϕ_l .

Figure 14 elucidates how Minkowski tensors can help discern some of the

morphological differences between the different hard sphere phases: first, this analysis of the average cell anisotropy clearly discerns the distinct geometries between the static jammed packings and the (also disordered) equilibrium fluid configurations and, more expectantly, the differences to the equilibrium ordered phase. Computing $\langle \beta_0^{2,0}(\phi_l) \rangle$ provides a signature of the origin of the data sets, clearly discerning the structure of equilibrium hard spheres and of the static jammed packings.

Second, the functional form $\langle \beta_0^{2,0}(\phi_l) \rangle$ is the same for six jammed static configurations shown here. These data sets comprise different global packing fractions and preparation protocols, including tomography data of dry acrylic beads [97] and glass beads settled against a fluid current [97], as well as Lubachevsky-Stilinger simulations of frictionless particles without gravity [98] and discrete element method simulations of spheres with friction and gravity [99]. This suggests a universality of the jammed static disordered spheres, in the sense of the following observation: the typical shape (quantified by $\beta_0^{2,0}$) of a Voronoi cell of a given local packing fraction ϕ_l is the same for all packings, regardless of protocol and of the global packing fraction ϕ_g . Note that this is in stark contrast to the case of the equilibrium fluid or ordered phase, where particularly small cells in a globally denser packing are more isotropic with larger $\beta_0^{2,0}$ than the same size cell in a looser packing. This result suggests that the global packing fraction of a jammed static disordered sphere packing is the result of combining typical “building blocks” with a given local ϕ_l in different proportions. This observation may go some way towards clarifying why random close packing of spherical particles appears to be largely protocol-independent.

Figure 14 has provided a test case where Minkowski tensors concisely discern the differences between two types of amorphous structures, in a quantitative fashion with an intuitive geometric real-space interpretation. The characterisation of amorphous cellular shapes is also relevant in various other contexts, e.g. for the relationship between structure and dynamics in glass-forming liquids [100] or for packing entropy of the hard micellar cores in supramolecular micellar materials [101], and for the understanding of physical properties of foams, including rheological [102] and static [103] properties and the evolution under ageing or coarsening [44, 104]. Minkowski tensors can be applied to these systems in an analogous fashion to the analysis of this section.

4. Conclusion and Outlook

This article provides the theoretical description and explicit algorithms for the use of Minkowski tensors in spatial structure and morphology characterisation in the natural sciences. Minkowski tensors, defined on the rigorous basis of integral geometry and endowed with strong statements about completeness, additivity and continuity, are natural extensions of the scalar Minkowski functionals. Because of their tensorial nature, Minkowski tensors allow for a quantitative evaluation of *shape* of anisotropic and orientation-dependent morphologies, on all length scales.

While the most fundamental definition of both scalar and tensorial Minkowski functionals is based on measure theoretic concepts from integral geometry [24], an alternative but equivalent definition based on curvature-weighted surface integrals is more intuitive for the reader without a background in measure theory. This approach also lends itself directly to numerical discretisation, resulting in the fast linear-time algorithms derived in this article. These algorithms have been comprehensively described and theoretically validated here for all relevant Minkowski tensors up to rank two, but can be generalised also for higher rank. An implementation of the algorithms described here is available as supplementary material, see below.

Minkowski tensors are versatile tools to quantitatively characterise morphological aspects related to orientation, anisotropy and elongation. Applications can be conceived in diverse fields, from nanostructures in softmatter to large-scale structures e.g. in background radiation sky maps [105].

For particulate assemblies such as granular matter or structural glasses, our previous analyses of random jammed sphere packing systems [1, 7] have contributed to clarifying the onset of order near the random close packing transition for spherical particles. Beyond this identification of order in these amorphous packings, Minkowski tensors lend themselves to the more complex task of quantitatively evaluating the structural changes in evolving amorphous packings, that never reach a state even with partial order, see also the discussion in sect. 3.2. In this context, the relationship between the Minkowski tensors and the bond orientational order parameters, defined by Steinhardt *et al* [106] as the lowest-order rotation invariants of the moments of a multipole expansion of the orientational distribution of nearest-neighbour bonds, leads to new insight into this question. We have already demonstrated that a simple idea based on Minkowski tensor analysis can remedy some of the drawbacks of the bond orientational order parameters, leading to robust *Minkowski structure metrics* [92]. A formal correspondence has been shown between the Minkowski tensors $W_1^{0,n}$ of rank $n = 0, 1, 2, \dots$ and the set of bond orientational order parameters [107, 108]. This provides geometric interpretation for both methods, e.g. the fact that $\beta_1^{0,2}$ and q_2 represent the same morphological information, see Fig. 5 in [92]. This motivates a more general study also for the other Minkowski tensors such as the curvature-weighted tensors $W_\nu^{0,n}$.

A second aspect that emphasises the usefulness of Minkowski tensors for particulate matter concerns the case of aspherical particles, such as tetrahedra and polyhedra, ellipsoids and super-ellipsoids, etc, all of which have received attention in recent studies [109, 110, 111, 112, 113]. In contrast to measures based on nearest-neighbour bonds, the Minkowski analysis naturally applies to these aspherical and possibly polydisperse particles, provided the Voronoi diagram is suitably defined. For example, with all tools in place for imaging experimental ellipsoid packings [114] and determining their Voronoi diagrams [115], the Minkowski tensor analysis may shed light on the more complicated, possibly less universal, mechanisms involved in jamming of ellipsoidal particles.

These results and the Minkowski tensor analysis itself are likely to provide new

insight also for other problems in particulate systems where spatial structure largely determines physical properties, such as static and rheological properties of glass-forming systems or liquids out of equilibrium.

Importantly, however, Minkowski tensor analysis is not restricted to particulate systems. To name one further example, Minkowski tensors can aid anisotropy or alignment studies of porous materials, cellular structures and other structures that consist essentially in a single connected component that percolates macroscopically, see also section 3.1. In addition to the use of Minkowski tensors as robust tools to extract anisotropy and morphology measures from tomographic or confocal microscopic images [4, 85], these measures may also be amenable to analytical treatment for some important mathematical models of porous materials. In particular for the case of the anisotropic Boolean model, it is feasible to obtain analytic expressions for the mean values of the translation-invariant Minkowski tensors $W_1^{0,2}$ and $W_2^{0,2}$ [116]. For ordered porous structures, analytic formulae for the Minkowski tensors of triply-periodic minimal surfaces have been derived from the Weierstrass parametrisation [5]. The feasibility of at least some analytic treatment hints at the role that the Minkowski tensors can play for an improved understanding of the spatial structure of porous materials, and in particular its formation by percolation processes.

The two-fold exploration of Minkowski tensors, on the one hand in terms of measure theory and on the other in terms of surface integrals, is a genuine scientific achievement of this article and of significant potential for future research. The mathematical disciplines of integral geometry [24] and stochastic geometry [117] are rich but (for non-experts) murky fishing grounds for research in random disordered systems. Many of the theorems relating to Minkowski functionals may well turn out to have physical counterparts or applications, following the examples of Hadwiger's theorem (that has been explored to describe shape dependence of the thermodynamics of confined fluids [19]) and the kinematic formula (needed for the development of density functionals for structured liquids [12]). There are several current trends in integral and stochastic geometry with potential for physical applications. For example, the so-called *mixed functionals* are generalisations of the Minkowski functionals to functionals of two (or more) bodies, obtained by integration over two-body support measures, see chapter 6.4 in [24]. The mixed measures are of likely benefit for the development of density functionals for fluids of aspherical particles without adjustable parameters. Current density functionals for non-spherical particles contain the ill-determined so-called ζ -factor, which results from only retaining the first term of an expansion [118]. For aspherical particles, this expansion is needed as it leads to a factorisation into measures centred on a single body of the double integration over the translational and orientational degrees of freedom of the relative position of *two* fluid particles. Future work on advanced methods to evaluate mixed measures may help avoid the need for this expansion, and lead to a deeper understanding of the geometric principles that govern the thermodynamic properties of aspherical fluids. By making the concise but, for many, unfamiliar notation of integral

geometry accessible to the reader, this article may facilitate future applications of integral geometry in physics and material science.

How do you measure the “shape” of an amorphous structure? This question expresses the need to identify a small number of morphological measures or structure metrics that, when evaluated for a spatial structure, capture its essential features in a few numbers. Which features are essential evidently depends on the physical property of interest, so a universal, generally valid answer to this question of the best structure metrics cannot be given. Nevertheless, some morphological properties recurrently appear as relevant to many physical processes. Some of these, such as densities or occupied volumes, areas of interfacial surfaces or spatial connectedness, turn out to be closely related to the scalar Minkowski functionals. The study of such quantities within an encompassing mathematical framework (here the theory of valuations in integral geometry) often gives new insight for the morphological analysis of the physical system; for example, the discussion of the relationship between d -dimensional percolation and the Euler index χ in the context of Minkowski functionals and integral geometry [119, 120] has contributed to the increasingly wide-spread use of χ as a measure of spatial connectedness in the physical sciences. The family of *tensorial* Minkowski functionals, at the heart of this article, have several properties that make them suitable generic shape measures to capture morphological aspects related to anisotropy, elongation and orientation: they are a natural generalisation of the concepts of volume and surface area to tensor-valued quantities, benefit from a definition widely applicable to different types of geometry and from significant mathematical theory, and are closely related to two already widely used tensors, namely the tensor of inertia and the interface tensor. We anticipate that these tensorial shape measures will be identified as the relevant morphological descriptors in a growing variety of physical systems. The analytical and algorithmic methods derived in this article will provide the tools for wide-spread use of Minkowski tensors analyses in physics, material science, biological imaging and other disciplines.

Supplementary online material and software

Software to compute the Minkowski tensors is made available as supplementary material to this article. The software and possible future extensions are also available through the website www.theorie1.physik.fau.de/karambola.

Acknowledgement

We are grateful to T. Aste, G. Delanay, M. Saadatfar, T. Senden and M. Schröter for the bead pack data, to J. Liu and D.A. Weitz for the actin biopolymer data, and M. Spanner for Monte Carlo data of equilibrium hard sphere systems. We thank C. Marlow for permission to reproduce his painting “White Spirits”, A. Boyde for the trabecular bone

image, M. Saadatfar for the metal foam image and A. Böker and V. Oszowka for the copolymer film image in Fig. 1. We thank J. Hörmann and M. Klatt for their critical comments on the manuscript, and M. Hoffmann for help with Voronoi computations. GEST, DH and KM acknowledge support by the German research foundation (DFG) through the research group ‘Geometry and Physics of Spatial Random Systems’ under grants SCHR1148/3-1, ME1361/12-1 and HU1874/2-1.

Appendix: Specific examples

For some simple shapes the rank-2 MT can be calculated analytically by using explicit surface parametrisation and expressions for surface normals and principal curvatures. Specifically for a sphere of radius R centred at the origin, one obtains

$$W_0 = \frac{4\pi}{3}R^3, \quad W_0^{2,0} = \frac{4\pi}{15}R^5Q \quad (46)$$

and, for $\nu = 1, 2, 3$ and $r + s = 2$,

$$W_\nu = \frac{4\pi}{3}R^{3-\nu}, \quad W_\nu^{r,s} = \frac{4\pi}{9}R^{3-\nu+r}Q \quad (47)$$

with the unit tensor Q .

For a convex polytope P , we write $\mathcal{F}_\mu(P)$ for the set of μ -dimensional faces of P , $\mu = 0, 1, 2$, that is, $\mathcal{F}_0(P)$ is the set of vertices, $\mathcal{F}_1(P)$ is the set of (*non-oriented*) edges, and $\mathcal{F}_2(P)$ is the set of faces. If $F \in \mathcal{F}_\mu(P)$, then we denote by $\mathbf{n}(P, F)$ the set of exterior unit normal vectors of P at F , which is a $(2 - \mu)$ -dimensional subset of the unit sphere \mathbb{S}^2 . Then we obtain, as a special case of general formulae in section 1.2,

$$W_\nu^{r,s}(P) = \frac{1}{3} \sum_{F \in \mathcal{F}_{3-\nu}(P)} \int_F \mathbf{x}^r \mathcal{H}^{3-\nu}(\mathrm{d}\mathbf{x}) \int_{\mathbf{n}(P,F)} \mathbf{n}^s \mathcal{H}^{\nu-1}(\mathrm{d}\mathbf{n}) \quad (48)$$

with $\nu = 1, 2, 3$. For the notation see the main text at eq. (17).

For a cuboidal box of dimensions $a_x \times a_y \times a_z$ aligned with the coordinate axes and centred at the origin eq. (48) yields $W_0 = a_x a_y a_z$, $W_1 = \frac{2}{3}(a_x a_y + a_y a_z + a_z a_x)$, $W_2 = \frac{\pi}{3}(a_x + a_y + a_z)$, $W_3 = \frac{4\pi}{3}$, $W_\nu^{1,0} = 0$ and all MT of rank two are diagonal matrices with the following entries

$$(W_0^{2,0})_{ii} = \frac{1}{12}a_i^3 a_j a_k, \quad (49)$$

$$(W_3^{2,0})_{ii} = \frac{\pi}{3}a_i^2, \quad (50)$$

$$(W_1^{2,0})_{ii} = \frac{a_i^3(a_j + a_k)}{18} + \frac{a_i^2 a_j a_k}{6}, \quad (51)$$

$$(W_1^{0,2})_{ii} = \frac{2a_j a_k}{3}, \quad (52)$$

$$(W_2^{2,0})_{ii} = \frac{\pi}{36}(a_i^3 + 3a_i^2(a_j + a_k)), \quad (W_2^{0,2})_{ii} = \frac{\pi}{6}(a_j + a_k) \quad (53)$$

where $\{i, j, k\} = \{x, y, z\}$ and permutations thereof.

A torus centred at the origin with major radius R_1 and minor radius $R_2 \leq R_1$ can be parametrised by $\mathbf{x}(u, v) = \{\cos(u) (R_1 + R_2 \cos(v)), \sin(u) (R_1 + R_2 \cos(v)), R_2 \sin(v)\}$ with $\alpha, \beta \in [0, 2\pi)$. The scalar functionals are explicitly given by $W_0 = 2\pi^2 R_1 R_2^2$, $W_1 = \frac{4\pi}{3} R_1 R_2$, $W_2 = \frac{2\pi^2}{3} R_1$ and $W_3 = 0$ and the vectorial measures are $W_\nu^{1,0} = 0$. The tensors of rank two are diagonal with degenerate eigenvalues $(W_\nu^{r,s})_{xx} = (W_\nu^{r,s})_{yy}$; the entries are given by

$$\begin{aligned} (W_0^{2,0})_{xx} &= \frac{\pi^2}{4} R_1 R_2^2 (4R_1^2 + 3R_2^2), & (W_0^{2,0})_{zz} &= \frac{\pi^2}{2} R_1 R_2^4 \\ (W_1^{2,0})_{xx} &= \frac{\pi^2}{3} R_1 R_2 (2R_1^2 + 3R_2^2), & (W_1^{2,0})_{zz} &= \frac{2\pi^2}{3} R_1 R_2^3 \\ (W_2^{2,0})_{xx} &= \frac{\pi^2}{6} R_1 (2R_1^2 + 5R_2^2), & (W_2^{2,0})_{zz} &= \frac{\pi^2}{3} R_1 R_2^2 \\ (W_3^{2,0})_{xx} &= \frac{2\pi^2}{3} R_1 R_2, & (W_3^{2,0})_{zz} &= 0 \\ (W_1^{0,2})_{xx} &= \frac{\pi^2}{3} R_1 R_2, & (W_1^{0,2})_{zz} &= \frac{2\pi^2}{3} R_1 R_2 \\ (W_2^{0,2})_{xx} &= \frac{\pi^2}{6} R_1, & (W_2^{0,2})_{zz} &= \frac{\pi^2}{3} R_1. \end{aligned}$$

For an ellipsoid given by $(x/l_x)^2 + (y/l_y)^2 + (z/l_z)^2 = 1$ the surface integrals all result in elliptic integrals and cannot be expressed in closed form. However, the scalar MF W_0 is $W_0 = \frac{4\pi}{3} l_x l_y l_z$. The MT $W_0^{2,0}$ is diagonal with

$$(W_0^{2,0})_{ii} = \frac{4\pi}{15} l_i^3 l_j l_k \quad (54)$$

where $\{i, j, k\}$ is $\{x, y, z\}$ and permutations thereof. The integration of all other tensors is easily numerically obtained by use of the ellipsoid parametrisation $\mathbf{x}(u, v) = \{l_x \cos(u) \sin(v), l_y \sin(u) \sin(v), l_z \cos(v)\}$ which yields explicit expressions for the metric tensor of the ellipsoidal surface, the normal vector, and the mean and Gaussian curvatures. These are readily integrated numerically. Fig. 15 shows the minimal to maximal eigenvalue ratio of the MT of rank two of ellipsoids with $l_x = 1$ and $1 \geq l_y \geq l_z$.

References

- [1] G.E. Schröder-Turk, W. Mickel, M. Schröter, G.W. Delaney, M. Saadatfar, T.J. Senden, K. Mecke, and T. Aste. Disordered spherical bead packs are anisotropic. *Europhys. Lett.*, 90:34001, 2010.
- [2] S.C. Kapfer, W. Mickel, F.M. Schaller, M. Spanner, C. Goll, T. Nogawa, N. Ito, K. Mecke, and G.E. Schröder-Turk. Local anisotropy of fluids using Minkowski tensors. *J. Stat. Mech.: Theory E.*, 2010(11):P11010, 2010.
- [3] Gerd E. Schröder-Turk, Varslot Trond, Liliana De Campo, Sebastian C. Kapfer, and Walter Mickel. A bicontinuous mesophase geometry with hexagonal symmetry. *Langmuir*, 27(17):10475–10483, 2011.
- [4] G.E. Schröder-Turk, W. Mickel, S. C. Kapfer, M. A. Klatt, F. M. Schaller, M. J. F. Hoffmann, N. Kleppmann, P. Armstrong, A. Inayat, D. Hug, M. Reichelsdorfer, W. Peukert, W. Schwieger, and K. Mecke. Minkowski tensor shape analysis of cellular, granular and porous structures. *Adv. Mater.*, 23:2535–2553, 2011.
- [5] W. Mickel, G.E. Schröder-Turk, and K. Mecke. Tensorial minkowski functionals of triply periodic minimal surfaces. *Interface Focus*, 2(5):623–633, 2012.

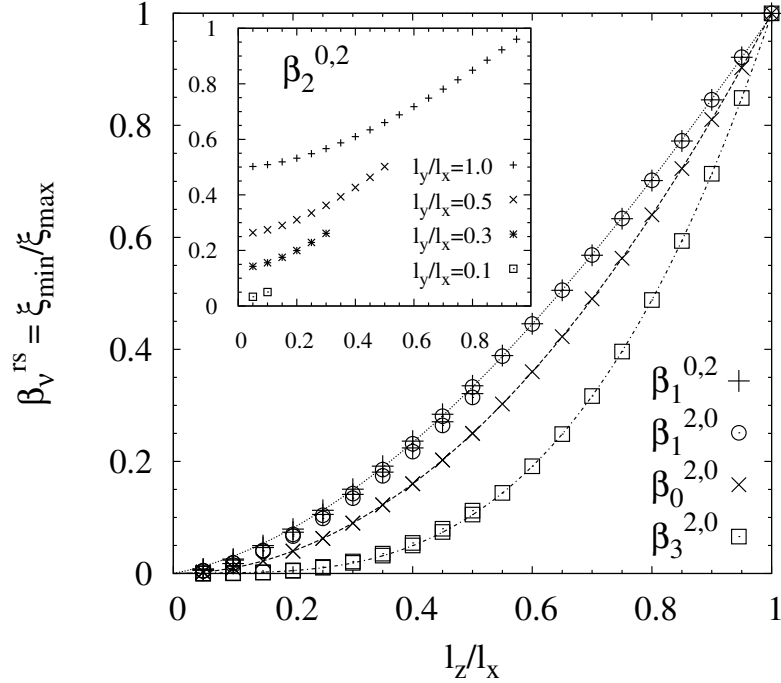


Figure 15. Eigenvalue ratio of the smallest and largest eigenvalues ξ_{\min} and ξ_{\max} of the MT $W_V^{r,s}$ of an ellipsoid with radii $l_x = 1$ and $l_x = 1 \geq l_y \geq l_z$ as function of $r = l_z/l_x$. Each symbol in the main plot represents data (hardly distinguishable) for three different intermediate radii $l_y = 0.1, 0.5, 0.9$ indicating that for these four tensors the minimal to maximal eigenvalue ratio is approximately the same for all values of the intermediate radius. The solid curves are fits to the data giving $\beta_3^{2,0} \approx 1.210r^3 - 0.235r^2 + 0.024$, $\beta_0^{2,0} = r^2$, $\beta_1^{2,0} \approx \beta_1^{0,2} \approx -0.366r^3 + 1.222r^2 + 0.139r$. The insert shows the eigenvalue ratio of the tensor $W_2^{0,2}$ as function of l_z/l_x . In contrast to the above four tensors, this ratio depends strongly on the value of the intermediate radius l_y . In particular, for $l_z = 0$ the eigenvalue ratio only becomes zero if the intermediate radius is also $l_y = 0$. For the maximal $l_y = 1$ the eigenvalue ratio converges to 0.5 for $l_z/l_x \rightarrow 0$.

- [6] G.E. Schröder-Turk, S.C. Kapfer, B. Breidenbach, C. Beisbart, and K. Mecke. Tensorial Minkowski functionals and anisotropy measures for planar patterns. *J. Microsc.*, 238:57–74, 2010.
- [7] S.C. Kapfer, W. Mickel, K. Mecke, and G.E. Schröder-Turk. Jammed spheres: Minkowski tensors reveal onset of local crystallinity. *Phys. Rev. E*, 85:030301, 2012.
- [8] V. Olszowka, M. Hund, V. Kuntermann, S. Scherdel, L. Tsarkova, A. Böker, and G. Krausch. Large scale alignment of a lamellar block copolymer thin film via electric fields: a time-resolved SFM study. *Soft Matter*, 2:1089–1094, 2006.
- [9] V. Olszowka, M. Hund, V. Kuntermann, S. Scherdel, L. Tsarkova, and A. Böker. Electric field alignment of a block copolymer nanopattern: direct observation of the microscopic mechanism. *ACS Nano*, 3:1091–1096, 2009.
- [10] M. Saadatfar, F. Garcia-Moreno, S. Hutzler, A.P. Sheppard, M.A. Knackstedt, J. Banhart, and D. Weaire. Imaging of metallic foams using X-ray micro-CT. *Colloid Surface A*, 344:107–112, 2009.
- [11] Contact details for Allan Boyde are a.boyde@qmul.ac.uk.

- [12] K. Mecke. Additivity, convexity, and beyond: Applications of Minkowski functionals in statistical physics. In Klaus Mecke and Dietrich Stoyan, editors, *Statistical Physics and Spatial Statistics – The Art of Analyzing and Modeling Spatial Structures and Patterns*, volume 554 of *Lecture Notes in Physics*, pages 111–184. Springer Verlag, 2000.
- [13] C. Arns, M.A. Knackstedt, and K. Mecke. Characterisation of irregular spatial structures by parallel sets and integral geometric measures. *Colloid Surface A*, 241(1–3):351–372, 2004.
- [14] K. Mecke and C.H. Arns. Fluids in porous media: a morphometric approach. *J. Phys.: Condens. Mat.*, 17:503–534, 2005.
- [15] C. Scholz, F. Wirner, J. Götz, U. Rude, G.E. Schröder-Turk, K. Mecke, and C. Bechinger. Permeability of porous materials determined from the euler characteristic. *Phys. Rev. Lett.*, 109:264504, 2012.
- [16] S. Rehse, K. Mecke, and R. Magerle. Characterization of the dynamics of block copolymer microdomains with local morphological measures. *Phys. Rev. E*, 77:051805, 2008.
- [17] J. Becker, G. Grün, R. Seeman, H. Mantz, K. Jacobs, K.R. Mecke, and R. Blossey. Complex dewetting scenarios captured by thin-film models. *Nat. Mater.*, 2:595–63, 2003.
- [18] K. Mecke. Morphological characterization of patterns in reaction-diffusion systems. *Phys. Rev. E*, 53(5):4794–4800, 1996.
- [19] P.-M. König, R. Roth, and K.R. Mecke. Morphological thermodynamics of fluids: Shape dependence of free energies. *Phys. Rev. Lett.*, 93(16):160601, 2004.
- [20] P.-M. König, P. Bryk, K. Mecke, and R. Roth. Curvature expansion of density profiles. *Europhys. Lett.*, 69:832–838, 2005.
- [21] H. Hadwiger. *Vorlesungen über Inhalt, Oberfläche und Isoperimetrie*. Springer, 1957.
- [22] G. Materon. *Random Sets and Integral Geometry*. Wiley, 1975.
- [23] L.A. Santaló. *Integral Geometry and Geometric Probability*. Addison-Wesley, 1976.
- [24] R. Schneider and W. Weil. *Stochastic and Integral Geometry (Probability and Its Applications)*. Springer, 2008.
- [25] J. Serra. *Image Analysis and Mathematical Morphology*. Academic Press, 1983.
- [26] H.J.A.M. Heijmans. *Morphological image operators*. Academic Press, 1994.
- [27] P. Soille. *Morphological Image Analysis – Principles and Applications*. Springer-Verlag, 1999.
- [28] H. Hansen-Goos and K. Mecke. Fundamental measure theory for inhomogeneous fluids of non-spherical hard particles. *Phys. Rev. Lett.*, 102:018302, 2009.
- [29] H. Hansen-Goos, R. Roth, K. Mecke, and S. Dietrich. Solvation of proteins: linking thermodynamics to geometry. *Phys. Rev. Lett.*, 99:128101, 2007.
- [30] S. Sporer, C. Goll, and K. Mecke. Motion by stopping: Rectifying Brownian motion of nonspherical particles. *Phys. Rev. E*, 78:011917, 2008.
- [31] C. Beisbart, M.S. Barbosa, H. Wagner, and L. da F. Costa. Extended morphometric analysis of neuronal cells with Minkowski valuations. *Eur. Phys. J. B*, 52(4):531–546, 2006.
- [32] C. Beisbart, R. Dahlke, K. Mecke, and H. Wagner. Vector- and tensor-valued descriptors for spatial patterns. In K. Mecke and D. Stoyan, editors, *Morphology of Condensed Matter - Physics and Geometry of Spatially Complex Systems*, volume 600 of *Lecture Notes in Physics*, pages 249–271. Springer, 2002.
- [33] S. Alesker. Description of continuous isometry covariant valuations on convex sets. *Geom. Dedicata*, 74:241–248, 1999.
- [34] D. Hug, R. Schneider, and R. Schuster. The space of isometry covariant tensor valuations. *St. Petersburg Math. J.*, 19:137–158, 2008.
- [35] H.R. Müller. Über Momente ersten und zweiten Grades in der Integralgeometrie. *Rend. Circ. Palermo (II. Ser.)*, 2(1):119–140, 1953.
- [36] P. McMullen. Isometry covariant valuations on convex bodies. *Rend. Circ. Palermo*, 50:259–271, 1997.
- [37] B. Brunet-Imbault, G. Lemineur, C. Chappard, R. Harba, and C.-L. Benhamou. A new anisotropy index on trabecular bone radiographic images using the fast Fourier transform.

- BMC Medical Imaging*, 5(1):4, 2005.
- [38] M. Saitou and Y. Fukuoka. Stripe pattern formation in Ag-Sb co-electrodeposition. *Electrochim. Acta*, 50(25–26):5044–5049, 2005.
- [39] M. Tunák and A. Linka. Analysis of planar anisotropy of fibre systems by using 2D Fourier transform. *Fibres Text. East. Eur.*, 15(5–6), 2007.
- [40] D.A. Blackadder, R.W. Gray, and N.G. McCrum. The anisotropy of linear polyethylene single crystal mats. *J. Polym. Sci. Pol. Phys.*, 14:769–771, 1976.
- [41] I. S. Atanasov, J. H. Durrell, L. A. Vulkova, Z. H. Barber, and O. I. Yordanov. Statistical characterization of surface morphologies. *Physica A*, 371:361–367, 2006.
- [42] J.G. Berryman. Planar spatial correlations, anisotropy, and specific surface area of stationary random porous media. *J. Appl. Phys.*, 83(3):1685–1693, 1998.
- [43] A.M. Kraynik, D.A. Reinelt, and F. van Swol. Structure of random monodisperse foam. *Phys. Rev. E*, 67(3):031403, 2003.
- [44] M. E. Evans, J. Zirkelbach, G. E. Schröder-Turk, A. M. Kraynik, and K. Mecke. Deformations of platonic foam cells: Effect on growth rate. *Phys Rev E*, 2012.
- [45] M. Doi and T. Ohta. Dynamics and rheology of complex interfaces. I. *J. Chem. Phys.*, 95(2):1242–1248, 1991.
- [46] W.J. Whitehouse. The quantitative morphology of anisotropic trabecular bone. *J. Microsc.*, 101(2):153–168, 1974.
- [47] T.P. Harrigan and R.W. Mann. Characterization of microstructural anisotropy in orthotropic materials using a second rank tensor. *J. Mater. Sci.*, 19:761–767, 1984.
- [48] M.J. Wald, B. Vasilic, P.K. Saha, and F.W. Wehrli. Spatial autocorrelation and mean intercept length analysis of trabecular bone anisotropy applied to in vivo magnetic resonance imaging. *Med. Phys.*, 34(3):1110–1120, 2007.
- [49] L.M. Mathieu, T.L. Mueller, P.-E. Bourban, D.P. Pioletti, R. Muller, and J.-A. E. Manson. Architecture and properties of anisotropic polymer composite scaffolds for bone tissue engineering. *Biomaterials*, 27(6):905–916, 2006.
- [50] M.Y.M. Chiang, X. Wang, F.A. Landis, J. Dunkers, and C.R. Snyder. Quantifying the directional parameter of structural anisotropy in porous media. *Tissue Eng.*, 12(6):1597–1606, 2006.
- [51] D. Inglis and S. Pietruszczak. Characterization of anisotropy in porous media by means of linear intercept measurements. *Int. J. Solids Struct.*, 40(5):1243–1264, 2003.
- [52] R.A. Ketcham and T.M. Ryan. Quantification and visualization of anisotropy in trabecular bone. *J. Microsc.*, 213(2):158–171, 2004.
- [53] M. Aubouy, Y. Jiang, J.A. Glazier, and F. Graner. A texture tensor to quantify deformations. *Granul. Matter*, 5:67–70, 2003.
- [54] F. Graner, B. Dollet, P. Marmottant, and C. Raufaste. Discrete rearranging disordered patterns, part I: Robust statistical tools in two or three dimensions. *Eur. Phys. J. E*, 25:349–369, 2008.
- [55] G. Durand, F. Graner, and J. Weiss. Deformation of grain boundaries in polar ice. *Europhys. Lett.*, 67:1038–1044, 2004.
- [56] E. Janiaud and F. Graner. Foam in two-dimensional couette shear: a local measurement of bubble deformation. *J. Fluid Mech.*, 532:243–267, 2003.
- [57] J. Rataj and I. Saxl. Analysis of planar anisotropy by means of the Steiner compact. *J. Appl. Probab.*, 26(3):490–502, 1989.
- [58] Y.-J. Sung and R. Farnood. Characterizing anisotropy of the deterministic features in paper structure with wavelet transforms. *J. Ind. Eng. Chem.*, 13(2):225–230, 2007.
- [59] A. Odgaard, E.B. Jensen, and H.J. Gundersen. Estimation of structural anisotropy based on volume orientation. A new concept. *J. Microsc.*, 157(2):149–162, 1990.
- [60] L.M. Karlsson and L.M. Cruz-Orive. Stereological characterization of structural anisotropy of rolled steel. *Microsc. Microanal.*, 11(2):1680–1681, 2005.
- [61] Craig Marlow. White spirits. Painting oil on canvas, Contact: Craig Marlow, PO Box 698, Sigatoka, Fiji Islands, 2004.

- [62] J. Rataj and M. Zähle. Mixed curvature measures for sets of positive reach and a translative integral formula. *Geometriae Dedicata*, 57:259–283, 1995.
- [63] D. Hug, R. Schneider, and R. Schuster. Integral geometry of tensor valuations. *Adv. Appl. Math.*, 41:482–509, 2008.
- [64] R. Schneider. *Convex Bodies: The Brunn-Minkowski Theory*. Cambridge University Press, 1993.
- [65] P.-E. Danielsson. Euclidean distance mapping. *Computer Graphics and Image Processing*, 14:227–248, 1980.
- [66] M. Heveling, D. Hug, and G. Last. Does polynomial parallel volume imply convexity? *Math. Annal.*, 328:469–479, 2004.
- [67] D.L. Cohn. *Measure Theory*. Birkhäuser, 1993.
- [68] H. Amann and J. Escher. *Analysis III*. Springer-Online, 2009.
- [69] L.C. Evans and R.F. Gariepy. *Measure theory and fine properties of functions*. Studies in advanced mathematics. CRC Press, 1992.
- [70] M. Berg. *Computational geometry: algorithms and applications*. Springer, 2000.
- [71] CGAL, Computational Geometry Algorithms Library. <http://www.cgal.org>.
- [72] D.H. Eberly. *Game Physics*. Elsevier, 2004.
- [73] P. Krsek, G. Lukas, and R. R. Martin. Algorithms for computing curvatures from range data. In A. Ball, editor, *The Mathematics of Surfaces VIII*, pages 1–16, 1998.
- [74] M. Meyer, M Desbrun, M. Schröder, and A. P. Barr. Discrete differential-geometry operators for triangulated 2-manifolds. *Visualization and Mathematics III*, pages 35–57, 2003.
- [75] I. Chavel. *Riemannian geometry - a modern introduction*. Cambridge Univ. Press, 1996.
- [76] J. Liu, K.E. Kasza, G.H. Koenderink, D. Vader, C.P. Broedersz, F.C. MacKintosh, and D.A. Weitz. Microscopic origins of nonlinear elasticity of biopolymer networks. preprint, 2007.
- [77] M.L. Gardel, J.H. Shin, F.C. MacKintosh, L. Mahadevan, P. Matsudaira, and D.A. Weitz. Elastic behavior of cross-linked and bundled actin networks. *Science*, 304:1301–1305, 2004.
- [78] E. Cukierman, R. Pankov, D.R. Stephens, and K.M. Yamada. Taking cell-matrix adhesion to the third dimension. *Science*, 294:1708–1712, 2001.
- [79] John A. Pedersen and Melody A. Swartz. Mechanobiology in the third dimension. *Annals of Biomedical Engineering*, 33(11):1469–1490, 2005.
- [80] C. Min Ma and Milan Sonka. A fully parallel 3D thinning algorithm and its applications. *Computer Vision and Image Understanding*, 64(3):420–433, 1996.
- [81] T.-C. Lee, R.L. Kashyap, and C.-N. Chu. Building skeleton models via 3-d medial surface/axis thinning algorithms. *CVGIP: Graphical Models and Image Processing*, 56(6):462–478, 1994.
- [82] W.E. Lorensen and H.E. Cline. Marching cubes: A high resolution 3D surface construction algorithm. In *Computer Graphics (Proceedings of SIGGRAPH '87)*, volume 21 (4), pages 163–169, 1987.
- [83] W. Mickel, S. Münster, L.J. Jawerth, D.A. Vader, D.A. Weitz, A.P. Sheppard, K. Mecke, B. Fabry, and Gerd E. Schröder-Turk. Robust pore size analysis of filamentous networks from 3D confocal microscopy. *Biophys. J.*, 95(12):6072–6080, 2008.
- [84] B. Breidenbach. *Scalar and tensor-valued Minkowski functionals of spatially complex structures*. PhD thesis, Friedrich-Alexander Universität Erlangen-Nürnberg, 2007.
- [85] M. Saadatfar, M. Mukherjee, M. Madadi, G.E. Schröder-Turk, F. Garcia-Moreno, F.M. Schaller, S. Hutzler, A.P. Sheppard, J. Banhart, and U. Ramamurty. Structure and deformation correlation of closed-cell aluminium foam subject to uniaxial compression. *Acta Materialia*, 60(8):3604 – 3615, 2012.
- [86] T. Aste. Volume fluctuations and geometrical constraints in granular packs. *Phys. Rev. Lett.*, 96(1):018002, 2006.
- [87] A. Mehta and S.F. Edwards. Statistical mechanics of powder mixtures. *Physica A*, 157(3):1091–1100, 1989.
- [88] F. Zamponi. Packings close and loose. *Nature*, 453:606–607, 2008.
- [89] Zhao, Song-Chuan, Sidle, Stacy, Swinney, Harry L., and Schröder, Matthias. Correlation between

- voronoi volumes in disc packings. *EPL*, 97(3):34004, 2012.
- [90] C.B. Barber, D.P. Dobkin, and H. Huhdanpaa. The Quickhull algorithm for convex hull. *ACM Transactions on Mathematical Software*, 22(4):469–483, 1996.
- [91] A. Okabe, B. Boots, K. Sugihara, S.N. Chiu, and M. Okabe. *Spatial Tesselations: Concepts and Applications of Voronoi Diagrams*. John Wiley and Sons, 2nd edition, 2000.
- [92] W. Mickel, S.C. Kapfer, G.E. Schröder-Turk, and K. Mecke. Shortcomings of the bond orientational order parameters for the analysis of disordered particulate matter. *J. Chem. Phys.*, 138(4):044501, 2013.
- [93] G.E. Schröder-Turk, R. Schielein, S.C. Kapfer, F.M. Schaller, G.W. Delaney, T. Senden, M. Saadatfar, T. Aste, and K. Mecke. Minkowski tensors and local structure metrics: Amorphous and crystalline sphere packings. In *Proceedings of Powders&Grains 2013, Sydney, Australia*, 2013.
- [94] F.H. Stillinger and B.D. Lubachevsky. Crystalline-amorphous interface packings for disks and spheres. *J. of Stat. Phys.*, 73:497–514, 1993.
- [95] M. Jerkins, M. Schröter, H.L. Swinney, T.J. Senden, M. Saadatfar, and T. Aste. Onset of mechanical stability in random packings of frictional spheres. *Phys. Rev. Lett.*, 101:018301, 2008.
- [96] T. Aste, M. Saadatfar, and T.J. Senden. Local and global relations between the number of contacts and density in monodisperse sphere packs. *J. of Stat. Mech.: Theory & Experiment*, 2006(07):P07010, 2006.
- [97] T. Aste, T. Di Matteo, M. Saadatfar, T. J. Senden, M. Schröter, and H.L. Swinney. An invariant distribution in static granular media. *Europhys. Lett.*, 79(2):24003, 2007.
- [98] B.D. Lubachevsky, F.H. Stillinger, and E.N. Pinson. Disks vs. spheres: Contrasting properties of random packings. *J. Stat. Phys.*, 64:501–524, 1991.
- [99] G.W. Delaney, S. Inagaki, and T. Aste. Fine tuning DEM simulations to perform virtual experiments with three-dimensional granular packings. In *Lecture Notes in Complex Systems*, volume 8, pages 169–186. World Scientific, 2007.
- [100] F.W. Starr, S. Sastry, J.F. Douglas, and S.C. Glotzer. What do we learn from the local geometry of glass-forming liquids? *Phys. Rev. Lett.*, 89(12):125501, 2002.
- [101] P. Ziherl and R.D. Kamien. Soap froths and crystal structures. *Phys. Rev. Lett.*, 85(16):3528–3531, 2000.
- [102] A. Kabla and G. Debrégeas. Local stress relaxation and shear banding in a dry foam under shear. *Phys. Rev. Lett.*, 90(25):258303, 2003.
- [103] A.M. Kraynik, D.A. Reinelt, and F. van Swol. Structure of random foam. *Phys. Rev. Lett.*, 93(20):208301, 2004.
- [104] Robert I. Saye and James A. Sethian. Multiscale modeling of membrane rearrangement, drainage, and rupture in evolving foams. *Science*, 340(6133):720–724, 2013.
- [105] D. Göring, M.A. Klatt, C. Stegmann, and K. Mecke. Morphometric analysis in gamma-ray astronomy using Minkowski functionals. *Astron. Astroph.*, DOI: 10.1051/0004-6361/201321136, 2013.
- [106] P.J. Steinhardt, D.R. Nelson, and M. Ronchetti. Bond-orientational order in liquids and glasses. *Phys. Rev. B*, 28(2):784–805, 1983.
- [107] S. Kapfer. *Morphometry and Physics of Particulate and Porous Media*. PhD thesis, Friedrich-Alexander Universität Erlangen-Nürnberg, 2011.
- [108] W. Mickel. *Geometry controlled phase behavior in nanowetting and jamming*. PhD thesis, Université Lyon, 2011.
- [109] G.W. Delaney and P.W. Cleary. The packing properties of superellipsoids. *EPL (Europhysics Letters)*, 89:34002, 2010.
- [110] A. Haji-Akbari, M. Engel, A.S. Keys, X. Zheng, R.G. Petschek, P. Palffy-Muhoray, and S.C. Glotzer. Disordered, quasicrystalline and crystalline phases of densely packed tetrahedra. *Nature*, 462(7274):773–777, December 2009.

- [111] M. Neudecker, S. Ulrich, S. Herminghaus, and M. Schröter. Jammed frictional tetrahedra are hyperstatic. *accepted for publication in Phys. Rev. Lett*, arXiv:1202.6272, 2013.
- [112] W. Man, A. Donev, F.H. Stillinger, M.T Sullivan, W.B. Russel, D. Heeger, S. Inati, S. Torquato, and P.M. Chaikin. Experiments on random packings of ellipsoids. *Phys. Rev. Lett.*, 94(19):198001, 2005.
- [113] A. Donev, I. Cisse, D. Sachs, E. Variano, F.H. Stillinger, R. Connelly, S. Torquato, and P.M. Chaikin. Improving the density of jammed disordered packings using ellipsoids. *Science*, 303:990–993, 2004.
- [114] F.M. Schaller, M. Neudecker, M. Saadatfar, G. Delaney, K. Mecke, G.E. Schröder-Turk, and M. Schröter. Tomographic analysis of jammed ellipsoid packings. *accepted for publication in Proceedings of Powders&Grains, Sydney*, 2013.
- [115] F.M. Schaller, G.E. Schröder-Turk, and et al. An algorithm for set voronoi diagrams of three-dimensional assemblies of aspherical particles. *in preparation*, 2013.
- [116] J. Hörrmann, D. Hug, M. Klatt, and K. Mecke. Minkowski tensor density formulas for boolean models. *in preparation*, 2013.
- [117] D. Stoyan, W.S. Kendall, and J. Mecke. *Stochastic Geometry and its Applications*. John Wiley & Sons, Chichester, UK, 2nd edition, 1995.
- [118] H. Hansen-Goos and K. Mecke. Tensorial density functional theory for non-spherical hard-body fluids. *J. Phys.: Condens. Mat.*, 22:364107, 2010.
- [119] Klaus Mecke and S. Seyfried. Strong dependence of percolation thresholds on polydispersity. *Europhys. Lett.*, 58(1):28–34, 2002.
- [120] Richard A. Neher, Klaus Mecke, and Herbert Wagner. Topological estimation of percolation thresholds. *Journal of Statistical Mechanics: Theory and Experiment*, 2008(1):P01011 (14pp), 2008.